

Hardware-accelerated graph neural networks: an alternative approach for event-based audio classification and keyword spotting on SoC FPGA

KAMIL JEZIOREK and PIOTR WZOREK, The AGH University of Krakow, Poland

KRZYSZTOF BŁACHUT, The AGH University of Krakow, Poland

HIROSHI NAKANO, Graduate School of Science and Technology, Keio University, Japan

MANON DAMPFHOFFER and THOMAS MESQUIDA, CEA-List, Université Grenoble Alpes, France

HIROAKI NISHI, Graduate School of Science and Technology, Keio University, Japan

THOMAS DALGATY, CEA-List, Université Grenoble Alpes, France

TOMASZ KRYJAK, The AGH University of Krakow, Poland

As the volume of data recorded by embedded edge sensors increases, particularly from neuromorphic devices producing discrete event streams, there is a growing need for hardware-aware neural architectures that enable efficient, low-latency, and energy-conscious local processing. We present an FPGA implementation of event-graph neural networks for audio processing. We utilise an artificial cochlea that converts time-series signals into sparse event data, reducing memory and computation costs. Our architecture was implemented on a SoC FPGA and evaluated on two open-source datasets. For classification task, our baseline floating-point model achieves 92.7% accuracy on SHD dataset – only 2.4% below the state of the art – while requiring over 10 \times and 67 \times fewer parameters. On SSC, our models achieve 66.9–71.0% accuracy. Compared to FPGA-based spiking neural networks, our quantised model reaches 92.3% accuracy, outperforming them by up to 19.3% while reducing resource usage and latency. For SSC, we report the first hardware-accelerated evaluation. We further demonstrate the first end-to-end FPGA implementation of event-audio keyword spotting, combining graph convolutional layers with recurrent sequence modelling. The system achieves up to 95% word-end detection accuracy, with only 10.53 μ s latency and 1.18 W power consumption, establishing a strong benchmark for energy-efficient event-driven KWS.

CCS Concepts: • **Hardware** → **Hardware accelerators**; *Emerging technologies*; *Reconfigurable logic and FPGAs*; • **Computing methodologies** → **Speech recognition**; *Artificial intelligence*.

Additional Key Words and Phrases: reconfigurable logic, event-based audio processing, graph convolutional neural networks, neuromorphic audio sensor, artificial cochlea, keyword spotting

ACM Reference Format:

Kamil Jeziorek, Piotr Wzorek, Krzysztof Błachut, Hiroshi Nakano, Manon Dampfhofer, Thomas Mesquida, Hiroaki Nishi, Thomas Dalgaty, and Tomasz Kryjak. 2025. Hardware-accelerated graph neural networks: an alternative approach for event-based audio

Authors' Contact Information: [Kamil Jeziorek](mailto:kamil.jeziorek@agh.edu.pl), kjeziorek@agh.edu.pl; [Piotr Wzorek](mailto:piotr.wzorek@agh.edu.pl), p wzorek@agh.edu.pl, The AGH University of Krakow, Krakow, Poland; [Krzysztof Błachut](mailto:krzysztof.blachut@agh.edu.pl), kblachut@agh.edu.pl, The AGH University of Krakow, Krakow, Poland; [Hiroshi Nakano](mailto:hiroshi.nakano@west.sd.keio.ac.jp), nakano@west.sd.keio.ac.jp, Graduate School of Science and Technology, Keio University, Tokyo, Japan; [Manon Dampfhofer](mailto:manon.dampfhofer@cea.fr), Manon.DAMPFHOFER@cea.fr; [Thomas Mesquida](mailto:thomas.mesquida@cea.fr), thomas.mesquida@cea.fr, CEA-List, Université Grenoble Alpes, Grenoble, France; [Hiroaki Nishi](mailto:hiroaki.nishi@west@keio.jp), west@keio.jp, Graduate School of Science and Technology, Keio University, Tokyo, Japan; [Thomas Dalgaty](mailto:thomas.dalgaty@cea.fr), Thomas.DALGATY@cea.fr, CEA-List, Université Grenoble Alpes, Grenoble, France; [Tomasz Kryjak](mailto:tomasz.kryjak@agh.edu.pl), kryjak@agh.edu.pl, The AGH University of Krakow, Krakow, Poland.

Permission to make digital or hard copies of all or part of this work for personal or classroom use is granted without fee provided that copies are not made or distributed for profit or commercial advantage and that copies bear this notice and the full citation on the first page. Copyrights for components of this work owned by others than the author(s) must be honored. Abstracting with credit is permitted. To copy otherwise, or republish, to post on servers or to redistribute to lists, requires prior specific permission and/or a fee. Request permissions from permissions@acm.org.

© 2025 Copyright held by the owner/author(s). Publication rights licensed to ACM.

Manuscript submitted to ACM

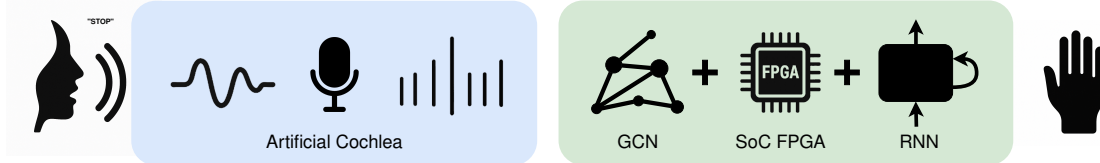


Fig. 1. In this work, we propose an event-based keyword spotting system in which speech signals are converted into asynchronous events by an artificial cochlea and represented as spectro-temporal event-graphs. These are processed by a GCN–RNN model deployed on a SoC FPGA, enabling low-power, low-latency, and efficient keyword spotting.

classification and keyword spotting on SoC FPGA. In *Proceedings of Make sure to enter the correct conference title from your rights confirmation email (Conference acronym 'XX)*. ACM, New York, NY, USA, 28 pages. <https://doi.org/XXXXXX.XXXXXXX>

1 Introduction

As the Internet of Things expands, distributed sensors are collecting ever-increasing quantities of data. This has driven the need for accurate and efficient computing systems capable of processing this data locally, for example, to make predictions [53]. The energy consumption and latency of these systems are of particular importance, as data is increasingly processed directly on edge devices, which operate under strict energy constraints (e.g. the battery of a smartwatch).

In most cases, the raw data produced by the sensors is time-series – continuous signals following the evolution of environmental variables [37]. For example, sensors that monitor the vibration of mechanical parts have been used to predict failures in gearboxes [57], or implantable cardioverter-defibrillators monitor the state of a patient’s heart in order to apply an electric shock in the event of dangerous fibrillation [21].

It is becoming increasingly common to use artificial intelligence (AI) methods to process this time-series data. However, using conventional hardware, such as GPUs (graphics processing units), consumes too much power, and microprocessors may struggle to meet the latency requirements of many applications. FPGAs (Field Programmable Gate Arrays) and custom integrated circuits offer a means of implementing architectures optimised to specific AI methods that are capable of meeting latency requirements while minimising power consumption [2, 3, 25]. Furthermore, it is necessary to apply the model at periodic intervals, and important temporal information present in the signal below the sampling frequency cannot be leveraged.

A particularly promising method is event-based AI, which operates on the sparse data generated by neuromorphic, event-based sensors and allows reducing power consumption and prediction latency [24]. Event-based sensors, instead of regularly sampling an environmental variable, generate “events” in case of the changes in the signal.

In this work, which is an extended version of our conference paper [45] presented at the *21st International Symposium on Applied Reconfigurable Computing*, we focus on audio signal processing. In this context, event-based time-series data is generated by a class of sensors known as artificial cochleas (AC) (also referred to as dynamic audio sensors or silicon cochleas) [38, 43]. Their operating principle is to apply a bank of band-pass filters to separate the signal into multiple frequency channels. A digital pulse (i.e. an event) is generated per channel in an asynchronous manner when the signal intensity changes by a pre-defined threshold. This results in a sparse spectrogram, which an event-based AI method exploits to perform efficient computation.

Processing AC-generated event-data has been the subject of many publications. The most common approach is to apply spiking neural networks (SNNs) implemented for specialised hardware [8, 17, 48]. However, it is not clear

how event-data sparsity can be truly exploited due to the nondeterministic pattern of synaptic weight-memory access [15, 19] inherent to SNNs.

Recently, event-graph neural networks have been proposed as an alternative way of processing event-data [16, 30, 36, 42, 52]. The event-graph approach consists of a dynamically updated graph generated by an event-sensor, and it involves applying graph convolutions on the resulting data structure. Unlike SNNs, the weight access pattern for many event-graph models is deterministic. This may provide an opportunity to develop new event-based AI hardware that is truly capable of exploiting the inherent sparsity of data to reduce power consumption and latency. Although digital architectures for accelerating event-graphs have been proposed in the context of computer vision [31, 64], a dedicated architecture for time-series audio applications has not yet been considered.

In this paper, we propose a hardware accelerator implemented on a SoC FPGA for event-graph audio classification and keyword spotting tasks (Figure 2). The proposed method enables real-time, end-to-end continuous processing while preserving the inherent sparsity of the input data. Specifically, we consider a recently proposed spectro-temporal model [52] developed for the classification of time-series data and evaluated on the Spiking Heidelberg Digits (SHD) dataset [13], which is a representative of time-series data.

We summarise our main contribution as follows:

- We use the hardware-aware design method to propose optimisations required to implement spectro-temporal event-graphs in reconfigurable hardware with low power, low latency and low resource utilisation. These optimisations include modifications to the graph generation module, the introduction of additional normalisation in graph convolution, and the careful selection of model hyperparameters.
- We propose the first embedded system for event-graph-based audio processing on a SoC FPGA and also the first hardware implementation that supports fully asynchronous event-by-event processing with conservation of data's temporal sparsity.
- We achieve a new state-of-the-art performance for time-series data classification on an FPGA applied to the Spiking Heidelberg Digits dataset, demonstrating significant improvements in resource utilisation, latency reduction and accuracy compared to previous SNN-based approaches. Moreover, we introduce the first FPGA-based benchmark results on the SSC dataset, establishing a reference point for future research.
- We propose the first end-to-end hardware implementation of the keyword spotting task model using event-based audio, designed for continuous and real-time processing. The architecture employs recurrent layers and achieves high word-end detection accuracy while maintaining low latency and efficient resource utilisation.

The remainder of this paper is organised as follows. In Section 2 we present an overview of the related work. In Section 3 we introduce the proposed modification and embedded audio processing system implementation. In Section 4 we present the results of ablation studies and comparisons with the state-of-the-art. We conclude with a discussion on future research directions and summary in Section 5.

2 Related work

2.1 Audio processing

In the domains of IoT devices and mobile robotics, there is a growing demand for efficient audio signal processing, particularly for the speech. One of the main tasks in this context is automatic speech recognition (ASR), which converts the entire speech segment into text. There are several techniques and datasets used for this task [1].

A special case of the ASR is keyword spotting (KWS), in which only specific, predefined words are recognised from a continuous speech. This makes KWS applications much smaller and computationally effective, as not all words need to be recognised. Therefore, they are increasingly used in embedded devices, microcontrollers, as e.g. voice assistants.

For many years, the most popular approach for this task was to use so-called mel-frequency cepstral coefficients (MFCC) [20] along with hidden Markov models (HMM) [54]. However, huge popularity of deep neural network-based approaches in various tasks motivated researchers to apply them in the audio domain as well, with the first work [11] published in 2014. Since then, NN-based solutions are much more widely used. For thorough overview of different KWS methods check an excellent paper [39].

The most popular dataset used for KWS development and evaluation is the publicly available Google Speech Command Dataset (GSCD) [62]. Its first version was released in 2017, while the second one year later, in which additional words and more speakers were added to extend the dataset. Currently, there are 35 words, over 100k speech segments and over 2600 different speakers. The recordings were made by smartphone and laptop microphones, they are therefore quite noisy. Currently, top solutions achieve over 98% accuracy on this dataset [32].

In this work, we distinguish between two related tasks: *word classification*, which identifies a given word based on a single audio sample without specifying its temporal occurrence, and *keyword spotting*, which detects and classifies a given word immediately after its occurrence, with the possibility of selecting a predefined set of keywords.

2.2 Event-audio data

Contrary to conventional microphones, which produce uniformly sampled waveforms, the artificial cochlea emits asynchronous events that capture temporal contrast in the acoustic scene. The invention of AC models, especially dynamic audio sensors (DAS) [38, 43], which are inspired by biological auditory systems, emerged an opportunity to apply event-based AI methods, extensively used in computer vision, for time-series applications.

The most widely used benchmark for evaluating event-based time-series models is the Spiking Heidelberg Digits (SHD) dataset [13]. It simulates an AC by filtering recordings with a computational model of the inner ear. The dataset comprises more than 10,000 recordings (8156 for training and 2264 for testing), consisting of spoken digits from zero to nine in both English and German. Each recording yields a sparse 700-channel spectrogram, with an average duration of 750 ms (Figure 6). In order to compare our SoC FPGA architecture of an event-graph neural network to previous state-of-the-art software and hardware implementations, we use the SHD dataset with the same train/test split.

The second benchmark employed is the Spiking Speech Command (SSC) dataset, derived from the Google Speech Commands Dataset (GSCD) by converting the recordings into spike-based representations [13], simulating the output of an event-based sensor, specifically an artificial cochlea. The dataset includes 75,466 training samples, 9,981 validation samples, and 20,382 test samples, covering 35 word categories spoken by a diverse set of speakers.

Existing works evaluated on both datasets mostly contain software implementations of recurrent spiking neural networks [6, 9, 13, 18, 55] and feed-forward models leveraging learned synaptic delays [14, 26, 40, 59, 68]. There are also articles [7, 50] devoted to comparison between DNNs and SNNs for keyword spotting applications with the latter around 4-5× more energy-efficient. The article [22] presents the usage of a neuromorphic auditory sensor (NAS), which is a digital version of artificial cochlea implemented in FPGA. The authors used its output to train and evaluate a spiking convolutional neural network on custom data. A very similar approach was taken by the authors of the work [63], in which the NAS sensor was also realised in FPGA and its output was used to train and evaluate an SNN on custom-generated events from the TIDIGITS dataset.

More recently, an alternative approach was proposed in [52], based on a fundamentally different paradigm. Instead of directly applying an SNN to the event stream, the data is first transformed into a graph representation and subsequently processed by a graph neural network (GNN). This event-graph neural network achieved performance comparable to state-of-the-art synaptic delay-based SNNs on the SHD benchmark, while requiring one to two orders of magnitude fewer synaptic weights in many cases. Notably, a compact model with only 17k parameters achieved a test accuracy exceeding 90%. These findings demonstrate the potential of event-graph methods for processing event-based time-series data. While it is believed that event-graphs, due to deterministic synaptic weight access patterns and natively asynchronous operation, may translate well into a dedicated hardware, it needs to be thoroughly investigated.

2.3 Event-audio processing on FPGA

Driven by the demand for real-time and low-power systems, numerous dedicated hardware implementations of event-based processing algorithms have been proposed on both application-specific integrated circuits [5] as well as FPGAs [35]. The majority of these works have focused on event-vision applications. To the best of the authors' knowledge, there are only two research papers describing FPGA-based SNN implementations for AC time-series processing [8, 41]. Both of them report benchmarking results on the SHD dataset and consider only the simple classification for samples containing single words.

The Spiker+ framework [8] and QUANTISENC tool [41] both target efficient SNN accelerators for FPGA-based edge computing, with Spiker+ achieving 72.9% accuracy on the SHD benchmark at 430 mW and 540 μ s latency, while QUANTISENC demonstrated 87.8% accuracy and 1.6 W peak power consumption.

This work is an extension of [45], where, drawing inspiration from the computer vision domain [31, 64], we introduced an event-graph neural network implemented on the Xilinx ZCU104 SoC FPGA for SHD audio classification with low latency and low power requirements. By leveraging a graph-based representation, we were able to drastically reduce the number of model parameters compared with state-of-the-art solutions, with only a marginal accuracy decrease (approximately 2%), thereby establishing new state-of-the-art results for FPGA-based event-audio processing.

Beyond event-based implementations, several works have explored FPGA accelerators for keyword spotting using conventional audio waveforms. In [67], a binary convolutional neural network (BCNN) was implemented on an Intel Cyclone V board, achieving 91.6% accuracy on the GSCD dataset. Similarly, a convolutional neural network (CNN) was deployed in [44] on a DE2-115 board with an Intel FPGA, reaching 90.4% accuracy on GSCD. In [34], a custom NN-based accelerator, RAMAN, was proposed for audio classification on the Microchip MPFS250T SoC FPGA, although no evaluation metrics were reported. Another study [46] implemented a separable CNN (SCNN) on a Digilent Arty A7-35T FPGA board, achieving over 90% accuracy on the MLPerf Tiny benchmark, though without reporting results on other datasets.

Given the promising potential of the event-graph approach, in this work we propose an end-to-end system based on graph convolutional neural networks for classification and keyword spotting tasks. We compare accuracy, power consumption, latency, and resource utilisation against prior FPGA-based implementations on publicly available benchmarks. This analysis enables us to assess whether the performance advantages of event-graph neural networks translate effectively to hardware for continuous real-time processing, and how they compare to SNN-based designs.

3 The proposed method

In this section we introduce our method for low-latency classification and keyword spotting that couple an artificial cochlea with an FPGA. We exploit the sparsity of this neuromorphic sensor with a hardware-aware design of a graph

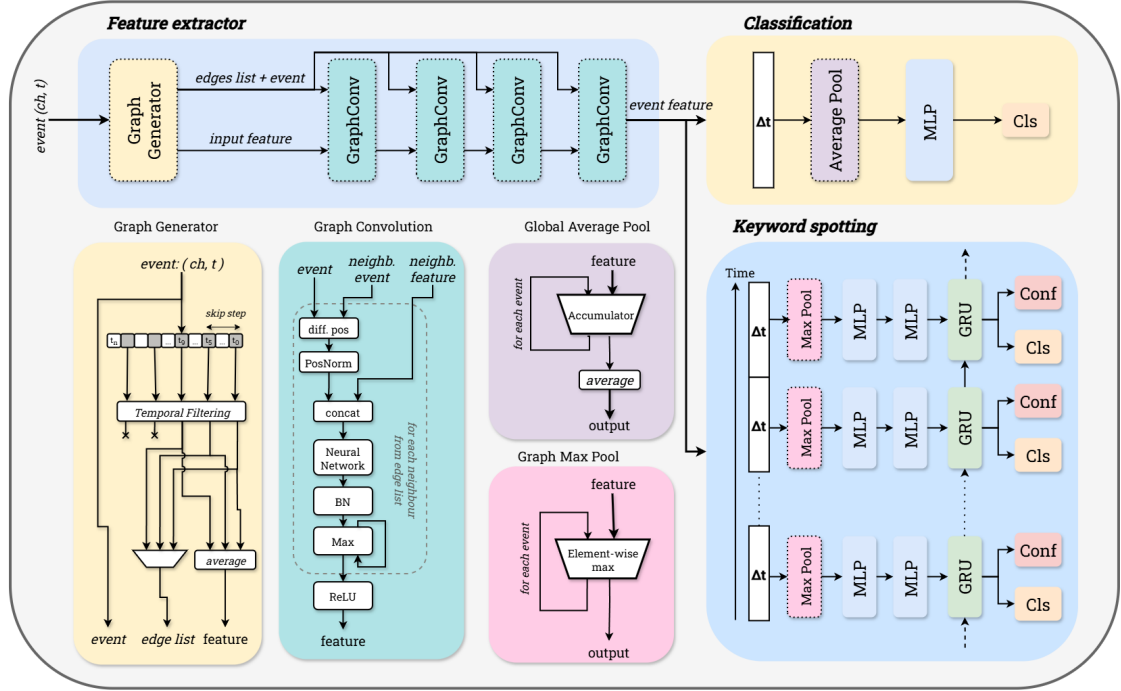


Fig. 2. Overview of our hardware-accelerated event-graph neural network implementation. Events from the artificial cochlea are first read and preprocessed in the processing system (PS), and subsequently processed by an asynchronous graph neural network in the programmable logic (PL). Modules marked with dotted lines operate on an event-by-event basis. For the classification task, we employ a global average pooling layer, which updates an accumulator over the entire sample and returns the result to a fully connected classifier (MLP). For keyword spotting, the data is divided into smaller time windows (Δt), aggregated using a graph max pooling operation, and processed sequentially by two MLPs and a GRU, after which confidence and class scores are computed. In both tasks, we employ the same feature extractor, consisting of a graph generator followed by four graph convolution layers.

convolutional network as a streaming feature extractor operating on event-derived graphs. The design minimises end-to-end latency and sustains constant throughput under bursty event rates. To generate a final prediction, we apply pooling across event embeddings from the last convolutional layer. The resulting vector is then fed into a network’s head, which produces the desired output for the processed event data.

As shown in Figure 2, classification and keyword spotting architectures share the same feature-extraction module but employ task-specific heads (which we describe in detail later).

3.1 Feature extraction

The principle of the event-graph approach is to generate a graph from raw events generated by an event-sensor – in this case the artificial cochlea. Formally, a graph is defined as $\mathcal{G} = (\mathcal{V}, \mathcal{E})$, where \mathcal{V} is the set of vertices and \mathcal{E} is the set of edges. Each vertex $v \in \mathcal{V}$ is associated with corresponding event’s position \mathcal{P} and feature vector \mathcal{X} , both of which characterise the underlying entity that the event represents, while edges represent the connections between pairs of these entities.

Spectro-temporal event-graphs are a specific form of event-graphs constructed from time-series data. They are typically created by performing a hemispherical search in the channel-time domain (Figure 6), establishing edges

between events that lie within defined distance. This neighbourhood can be determined by spatial and temporal radius thresholds, or, alternatively, edges can be assigned randomly within the search volume. Each new event generated by the sensor forms directed edges from previously recorded events found within a semi-circle defined by a channel radius r_{ch} and a time radius r_t . By employing this method, the graph can be updated for each new event and resulting vertex can be processed directly, eliminating the need for data aggregation within predefined time windows. This significantly reduces the overall system latency.

Given an event-graph, we can apply PointNetConv [10] operations across L convolutional layers. Each layer uses a unique weight matrix shared across all events. Within each layer, the following operation is performed to update the embedding of the i^{th} event:

$$\hat{X}_i = \max_{j \in \mathcal{N}(i)} (\phi([X_j \parallel (\mathcal{P}_j - \mathcal{P}_i)])), \quad (1)$$

where \hat{X}_i is the updated feature vector for event i , and $\phi(\cdot)$ represents a fully-connected layer. The notation \parallel indicates the concatenation of the feature vector X_j with the relative position vector $\mathcal{P}_j - \mathcal{P}_i$. After this transformation, a feature-wise max pooling aggregates the neighbour contributions into a single output vector per event, and a ReLU activation is applied to introduce nonlinearity.

The following subsections detail the adaptations and optimisations performed in order to map feature extraction baseline [52] to a hardware accelerator architecture on FPGA.

3.1.1 Graph generator. The baseline model presented in [52] has proven effective in capturing spectro-temporal relationships within event-graphs. However, significant challenges are faced when considering hardware implementation.

In [52], the feature vector X of each event consisted of two components of a normal vector estimated by fitting a local surface to the event-data using a least-squares approach. The position \mathcal{P} comprised a channel index and a timestamp. The relative positions between events defined edge vectors, creating an $\mathcal{N}(i)$ neighbourhood set for each node i .

However, the calculation of a normal vector requires fitting regression lines to the event-data that has a high computational complexity. Moreover, identifying neighbouring vertices requires storing all vertex vectors in memory and performing sequential searches, resulting in high latency and significant memory overhead.

To address these limitations, a novel graph generation method was designed to optimise memory usage, reduce latency, and minimise computational overhead. The following key modifications were introduced:

- (1) Drawing inspiration from FPGA-based event camera data processing implementations [31, 64], events are stored in 1D context memory (implemented as a block RAM memory (BRAM)) using their channel ch as the address and timestamps t as the data. Only the most recent event generated per channel is stored, continuously overwriting timestamps at each channel index. Each new event can be connected only to the ones already processed, creating a directed graph. The number of neighbours with the same channel ch is thus limited to 1, significantly reducing the required memory usage.
- (2) Event-normal vectors were replaced with simpler features based on the average timestamp and channel coordinates of neighbouring events, massively reducing the computational cost.
- (3) To improve the efficiency of neighbour search, we introduced a method called *skip step connection*. This corresponds to a pre-defined deterministic pattern regarding how edges can be formed between vertices.

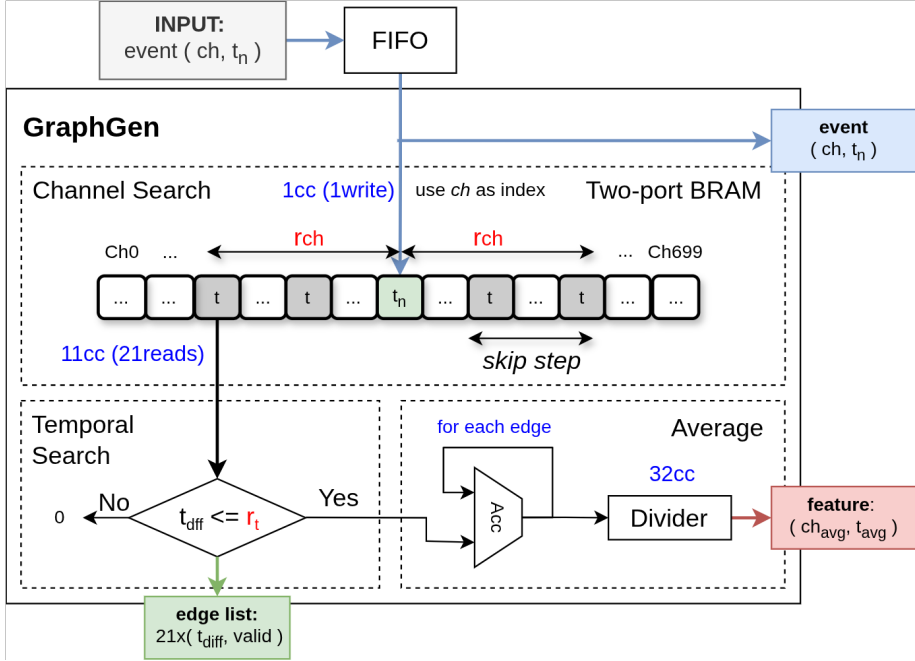


Fig. 3. Diagram of the graph generation hardware module, which takes events from FIFO as input, and outputs the vertex features along with the list of its edges. The blue colour indicates the time (measured in clock cycles) required for the individual steps.

Figure 3 illustrates the main components and data flow of the graph generation module. Asynchronous events, defined by their time t and channel index ch , enter a first-in first-out (FIFO) buffer, ensuring a stable data stream. Each event then moves to a 1D context memory indexed by the channel.

The module performs a neighbour search using the *skip step connection* method. Instead of scanning all possible neighbours, the system reads events at fixed intervals along the channel dimension from the BRAM. Events that meet the *temporal search* criteria (based on r_t radius) are added to an edge list, and their corresponding time and channel indices are fed into the accumulator. After iterating over all channels, this accumulator computes the average position of the neighbours using a simple divider. The resulting averaged features, together with the newly stored event and the edge list, are then passed to the first stage of the graph convolution pipeline.

The total number of clock cycles N_{cycles} required for graph generation depends on the channel radius (r_{ch}), the *skip step* (s), and the additional cycles for feature computation (N_{div}). Assuming dual-port memory (two reads per clock cycle), this can be expressed as:

$$N_{cycles} = \frac{1 + 2 \cdot \frac{r_{ch}}{s}}{2} + N_{div} \quad (2)$$

Here, 1 corresponds to the central channel read, $2 \cdot \frac{r_{ch}}{s}$ represents the reads from the upper and lower channels, and N_{div} accounts for division. In our implementation (designed based on ablation studies described in Section 4.2) we selected the radius r_{ch} of 100 with *skip step* s of 10.

3.1.2 Graph convolution. In the baseline approach, the PointNetConv [10] convolutional layer was used, which extends the classical *message passing mechanism* commonly used in graph convolutions. As highlighted in [30, 31], Manuscript submitted to ACM

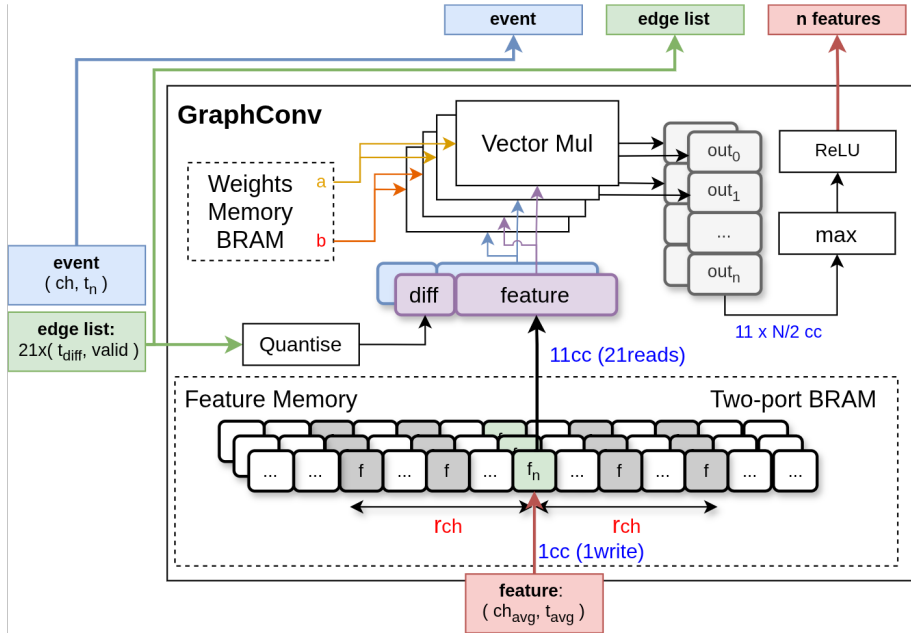


Fig. 4. Diagram of the graph convolution hardware module. The arrows indicate the dataflow in the module, while the blue text indicates the time (measured in clock cycles) required for the individual steps.

these layers are lightweight and well-suited for hardware acceleration, making them a natural choice for adoption in our work. However, we introduce two key modifications.

First, we integrate a *batch normalisation* (BN) layer into ϕ to ensure stable training. Notably, during quantisation these layers are folded [29], which prevents any increase in the model parameters for hardware deployment. The second and more important change involves an additional normalisation step for the positional differences used on the event-graph edges. The input data is initially normalised to $(0, 1)$ range, while neighbours are determined within the radius r_{ch} and r_t . Consequently, channel index differences are within $(-r_{ch}, r_{ch})$, and time index differences are within $(-r_t, 0)$ due to the use of a time-based directed graph generator. These values occupy only a small fraction of $(0, 1)$ range, which adversely affects training and reduces precision during quantisation. To address this, we apply *positional normalisation* (PN) after computing position differences, rescaling the values back to $(0, 1)$ range, by multiplying time differences by $-\frac{1}{r_t}$, and channel differences by adding r_{ch} and multiplying by $\frac{2}{r_{ch}}$.

The modified model is expressed as:

$$\hat{X}_i = \max_{j \in N(i)} (BN \phi([X_j || PN(\mathcal{P}_j - \mathcal{P}_i)])). \quad (3)$$

For hardware implementation each graph convolution assumes fully asynchronous event-by-event processing and can be executed in parallel. Each incoming event with its edge list and input features is processed independently. The module must also access the features of each vertex connected with an edge and the difference between the neighbour and the processed event. For this purpose, we implemented one 2-port BRAM memory that stores the features of the last processed event for each channel, and another one for storing the weights (see Figure 4).

To determine the final output feature, the linear layer must be applied for the vertex itself (so-called self-loop) and for each of its neighbours (a maximum of $\text{MAX_EDGE} = 21$ times with the $r_{ch} = 100$ and *skip step* $s = 10$). The key part of the graph convolution is the vector multiplication module – in order to reduce resource utilisation, the module was implemented in a way that some of the calculations were performed sequentially (inspired by [31]).

Taking advantage of two-port memories, we process two feature vectors and calculate two elements of the output vector at the same time (cf. Figure 4). The total number of clock cycles required to perform the convolution for a single event can be determined with the following formula:

$$N_{\text{cycles}} = \frac{\text{MAX_EDGE} + 1}{2} \cdot \frac{\text{OUT_DIM}}{2} \quad (4)$$

The graph convolution module can be considered a bottleneck of the proposed method. The throughput of the system is dependent on the maximum number of clock cycles required per single event. For our baseline model designed for classification and implemented for a 200 MHz clock, the theoretical throughput was thus calculated to be 555 kEPS (thousand events per second). At the same time, the average value in the SHD dataset is around 20 kEPS. However, it should be noted that the number of parallel vector multiplication modules could be increased to improve latency and throughput (using additional resources), or decreased with an opposite effect. This flexibility improves system scalability and applicability for different tasks and requirements.

An essential part of the system is the applied quantisation. In our work, all multiplications are performed exclusively on integer values with the bit precision that can be selected per layer. Both feature map elements and weights are stored in memory as unsigned integers, and rescaled before (quantisation) and after (re-quantisation) multiplications. For scaling, we use DSP multiplication and bit-shifting or look-up tables (depending on the number of possible quantised values) adhering to the methodology proposed in [29].

3.2 Classification

The first task addressed in this work is time-series classification. In this setting, an event-based data stream corresponding to the recording of a single word is provided to the system. The prediction is generated only after the entire sample has been fully processed. To achieve this, the event features are first aggregated using graph average pooling, and the resulting representation is then passed to a classifier for the final score.

3.2.1 Graph average pool. To obtain a compact representation of the event features produced by the graph convolution layers, a global graph pooling operation is applied. This step aggregates information from all events within a sample, reducing the representation to a single fixed-length vector that can be processed by fully connected layers. In the original approach [52], global average pooling was employed. By averaging the accumulated event features, the model captures a global summary that is particularly suitable for subsequent classification tasks. In our experiments (Section 4.2.3), we tested simpler alternatives such as global maximum pooling and global sum pooling; however, these methods led to a notable performance drop (by 7 pps for max pooling and 5 pps for sum pooling). Based on these findings, we retain the original average pooling strategy.

We implemented a global average pooling module which receives the features from the last stage of the graph convolution (Figure 2) to the input. The mean value is calculated by accumulating the sum of each vector feature in a given register. To determine the number of events that have been accumulated, a simple counter is used. When the output vector corresponding to the last event in a sample is calculated, the accumulator register values are divided by the current value of the counter. These values are then output by the module and stored in a BRAM memory.

3.2.2 Classification head. The pooled feature vector obtained from the global graph pooling layer is subsequently passed to a classification head. This module consists of a multi-layer perceptron (MLP), designed to map the compact representation into the target class space. The MLP applies two fully connected layers with ReLU activation functions. A softmax function is then used to normalise the output scores into class probabilities.

For FPGA-based hardware, we investigated two approaches for implementing the classification head. The first approach leverages the heterogeneous nature of the target platform by executing the multilayer perceptron within the processing system (PS) rather than the programmable logic (PL). Since the MLP is applied only after the entire input sequence has been processed by the graph neural network feature extractor, hardware acceleration is not critical at this stage. In this configuration, the MLP operates with full precision using floating-point arithmetic, without quantisation.

However, communication between the PS and PL introduces additional latency, and execution on the CPU increases energy consumption. To address these limitations, we also implemented the classification head within the reconfigurable PL. In this design, the MLP weights and activations are quantised to 8 bits, and computation is carried out using two vector-multiplication modules. This architecture was specifically chosen to efficiently exploit the double-port BRAM memory available for weight storage. A detailed evaluation and comparison of these two approaches is presented in Section 4.3.3.

3.3 Keyword spotting

While the simple classification task assumes that the entire word is contained within a single input sample, keyword spotting requires operating on a continuous event stream, where the offset of a word is not known in advance. In this scenario, the system must both detect the temporal boundaries of a spoken keyword and classify its content.

To address this challenge, the event stream is divided into smaller temporal windows. For each window, event features are extracted and pooled. These window-level features are then processed by a recurrent module, enabling the system to capture long-term temporal dependencies and to make predictions in an online manner.

3.3.1 Graph max pool. In contrast to the classification task, in keyword spotting the aggregation of events is performed over a significantly smaller temporal window Δt (1000 ms for classification vs 10 ms for KWS). As a result, the use of an element-wise operator has a less detrimental effect on performance. As demonstrated in the ablation studies (Section 4.2.3), the difference between applying average/add pooling and max pooling under these conditions is negligible, with a slight advantage for the max operation. Additionally, for hardware implementation, max pooling is preferable, since it eliminates the need for accumulation and division, and reduces the operation to a simple element-wise comparison and replacement. Therefore, in the keyword spotting task we adopt graph max pooling.

3.3.2 KWS head. The KWS head operates on a stream of pooled feature vectors computed over fixed-length windows of size Δt . Let $\{\mathbf{f}_t\}_{t=1}^T$ denote the sequence of window-level vectors (one per Δt window). Each \mathbf{f}_t is first transformed by a lightweight two-layer STEM with nonlinearities (ReLU), which improves local representation for temporal modelling. The STEM is intentionally shallow to minimise latency and resource usage.

For temporal modelling we employ a gated recurrent unit (GRU) [12], chosen as a compromise between model quality and resource utilisation. Vanilla RNNs are prone to vanishing gradients and insufficient temporal context modelling, while long short-term memory (LSTM) [27] networks, although often more accurate, incur higher parameter counts and latency due to an additional gate and explicit cell state updates.

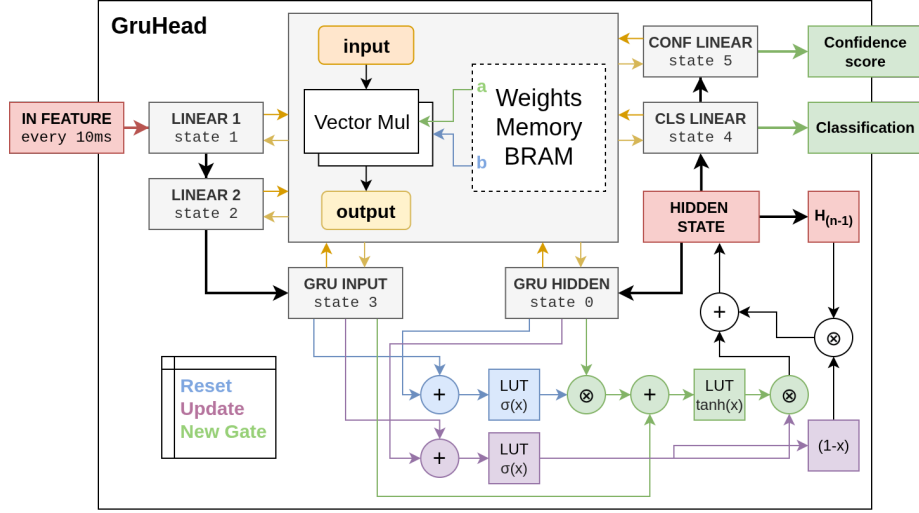


Fig. 5. Diagram of the head of the hardware KWS module. The key part of this module is vector multiplication shared between consecutive MLPs – its utilisation is controlled with the state machine.

Let \mathbf{x}_t be the STEM-transformed input at time t , and \mathbf{h}_{t-1} the previous hidden state. The GRU updates are:

$$\mathbf{z}_t = \sigma(W_z \mathbf{x}_t + U_z \mathbf{h}_{t-1} + \mathbf{b}_z), \quad (5)$$

$$\mathbf{r}_t = \sigma(W_r \mathbf{x}_t + U_r \mathbf{h}_{t-1} + \mathbf{b}_r), \quad (6)$$

$$\tilde{\mathbf{h}}_t = \tanh(W_h \mathbf{x}_t + U_h (\mathbf{r}_t \odot \mathbf{h}_{t-1}) + \mathbf{b}_h), \quad (7)$$

$$\mathbf{h}_t = (\mathbf{1} - \mathbf{z}_t) \odot \mathbf{h}_{t-1} + \mathbf{z}_t \odot \tilde{\mathbf{h}}_t, \quad (8)$$

where $\sigma(\cdot)$ denotes the logistic sigmoid function, \odot represents element-wise multiplication, and W, U, \mathbf{b} . are the learnable weight matrices and bias vectors associated with the reset gate (r), update gate (z), and candidate hidden state (h), respectively. The hidden state \mathbf{h}_t integrates features over time and is updated once per Δt window, enabling strictly online operation.

At each time step t , two outputs are produced from the current hidden state \mathbf{h}_t : (i) class probabilities (CLS), obtained through a linear transformation followed by a softmax activation, and (ii) a scalar confidence score (CONF), obtained through a linear transformation followed by a sigmoid activation. Consequently, every Δt window yields both a class prediction and an associated confidence estimate.

Given the significantly lower pooling times compared to the classification task (10 ms vs 1000 ms), efficient computation of the final prediction becomes highly desirable. Based on this observation, we implemented the KWS head in the programmable logic alongside feature extraction and pooling, in order to minimise latency and energy consumption.

The head of the hardware KWS module is organised as a state machine that sequentially controls the computations required for prediction (illustrated in Figure 5). Unlike the rest of the system, which is fully pipelined and optimised for parallel execution, this component employs a control-flow-oriented design. The core of the module consists of two vector multiplication units. They are used to efficiently exploit the dual-port memory available for weight storage; however, the level of parallelism can be adjusted – more units can be instantiated to reduce latency, while fewer units can

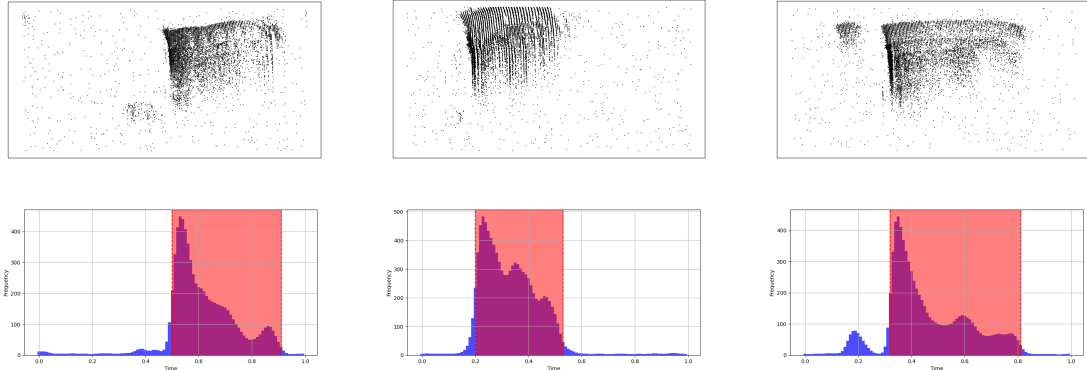


Fig. 6. Examples of spiking event stream with automatically extracted keyword boundaries. Top: raw spiking events; bottom: smoothed histogram with detected active range.

be used to save energy and FPGA resources. Each matrix multiplication required for prediction is performed sequentially (processing two rows in parallel), with the state machine orchestrating input reloading and output accumulation.

Using this scheme, the first and second MLPs of the STEM are computed in states 1 and 2, respectively. The hidden state \mathbf{h}_t is then updated according to the GRU recurrence equations, based on the previous hidden state \mathbf{h}_{t-1} and the STEM-transformed input \mathbf{x}_t . GRU-related multiplications (state 3) reuse the same resources as the STEM computations. Nonlinear functions, including the *sigmoid* and *tanh*, are implemented via look-up tables, while the Hadamard product is mapped to the FPGA's logic fabric. The updated hidden state is then passed through the classification and confidence score layers, again reusing the same multiplication resources (states 4 and 5). At this stage, the final prediction is generated and forwarded to the module output.

Finally, the hidden state is also supplied to the GRU MLP to compute the term $U\mathbf{h}_{t-1} + \mathbf{b}$ required for the next iteration (state 0). This step is also triggered once at the beginning of processing for initial \mathbf{h}_{t-1} (hence the state “0”). After each multiplication in the KWS head module, we apply re-quantisation following the methodology described in [29], implemented using the FPGA's DSP resources.

The proposed head implementation was designed to minimise resource utilisation. Since this operation is executed only once every 10 ms, the additional latency introduced by the sequential computations does not impose a significant delay on the overall system.

3.3.3 Data preparation. The original SHD and SSC datasets were designed for recognition tasks and therefore do not include time-aligned onset/offset annotations for individual keywords. To obtain labels suitable for keyword spotting, we derive segment boundaries from the continuous event stream by thresholding a *smoothed activity histogram* constructed on a *fixed temporal grid* with bin width Δt over a sample time window T .

Let $T > 0$ denote the per-sample duration, and let $\Delta t > 0$ be the histogram bin width (in milliseconds). We form $N = \lceil T/\Delta t \rceil$ bins with boundaries:

$$\text{bin_edges} = [0, \Delta t, 2\Delta t, \dots, N\Delta t] \cap [0, T], \quad (9)$$

and define $\mathbf{hist} \in \mathbb{R}^N$ as event counts per bin. Our objective is to estimate the active interval $[t_{\text{start}}, t_{\text{end}}] \subseteq [0, T]$ of the spoken keyword, which we then use as ground truth for KWS training and evaluation.

Table 1. Hyperparameters for Δt -binned KWS label extraction.

Quantity	Symbol/name	Default/example
Sample window	T	1 s (based on the sample)
Histogram bin width	Δt	10 ms
Gaussian kernel size (in bins)	k	7
High threshold	$T_{\text{high}} = \mu + \alpha\sigma$	$\alpha = 0.5$
Low threshold	$T_{\text{low}} = \beta T_{\text{high}}$	$\beta = 0.2$
Cooldown	<code>cooldown_steps</code> , $\tau_{\text{cool}} = \text{cooldown_steps} \cdot \Delta t$	5 bins
Min. duration	δ_{min}	40 ms

We first obtain a smoothed signal by convolving the raw histogram with a 1-D Gaussian kernel of length k in bins, which suppresses noise and micro-pauses:

$$\text{hist}^{(\text{smooth})} = \text{hist} * g_\sigma, \quad g_\sigma[m] \propto \exp\left(-\frac{m^2}{2\sigma^2}\right), \quad m \in \{-\frac{k-1}{2}, \dots, \frac{k-1}{2}\}. \quad (10)$$

On this smoothed trace, we compute *adaptive hysteresis thresholds*. The high threshold for activation is:

$$T_{\text{high}} = \mu + \alpha\sigma, \quad (11)$$

where μ and σ are the mean and standard deviation of $\text{hist}^{(\text{smooth})}$. The low threshold is a fraction of the high threshold, $T_{\text{low}} = \beta T_{\text{high}}$. This hysteresis gap stabilises detection across varying recording levels and mitigates rapid switching near the decision boundary.

Activation onset is defined as the first upward crossing of T_{high} . Once activated, the state remains active until `cooldown_steps` consecutive bins fall below T_{low} , implementing a cooldown of duration:

$$\tau_{\text{cool}} = \text{cooldown_steps} \cdot \Delta t, \quad (12)$$

which prevents a single keyword from being fragmented into multiple segments due to brief dips in activity. The deactivation time t_{end} is assigned to the corresponding bin edge. If the sequence reaches the end of the recording at T while still active, we set $t_{\text{end}} = T$. Under the single-keyword assumption, only the first such active interval is retained. Samples without any upward crossing of T_{high} are labelled as “no-keyword” (or excluded from training). Finally, extremely short detections are suppressed by enforcing a minimum duration:

$$(t_{\text{end}} - t_{\text{start}}) \geq \delta_{\text{min}}, \quad (13)$$

equivalently $\lceil \delta_{\text{min}} / \Delta t \rceil$ bins.

The resulting automatically derived onset/offset labels – visualised in Figure 6 – are used as ground truth for training and evaluating our KWS models. The best-performing hyperparameter settings, empirically validated for both SHD and SSC datasets, are summarised in Table 1.

4 Evaluation

4.1 Setup

All investigated models share a common feature-extraction backbone composed of four PointNetConv layers followed by a graph pooling layer (Section 3). For the classification task, the backbone is extended with a two-layer multilayer

perceptron classifier (Section 3.2.2). For the keyword spotting (KWS) task, the backbone is augmented with a two-MLP STEM preceding a gated recurrent unit (GRU) layer (Section 3.3.2). Two task-specific output heads are then attached: (i) a confidence head, which estimates the most likely onset timestep of the keyword within the input sequence, and (ii) a classification head, which assigns the detected segment to one of the C predefined classes. Taking inspiration from prior works that use the Google Speech Commands dataset for command classification, we divided the Spiking Speech Commands dataset into two subsets: SSC-35 and SSC-11. In SSC-35, all classes are considered relevant, while in SSC-11, only 10 target words (e.g. stop, go, off, right) are retained, with the remaining words grouped into an additional class labelled “unknown”.

All models were implemented in PyTorch [49] with the PyTorch Lightning framework [23]. For the classification task, the training was performed using a standard cross-entropy loss applied to the classifier outputs. For the KWS task, a multitask learning strategy was employed. The confidence head was trained using a weighted binary cross-entropy loss over all timesteps, where the positive class was weighted by the ratio of negative to positive samples (99 : 1) to mitigate severe class imbalance. The classification head was trained exclusively at the timestep corresponding to the maximum confidence score, using a cross-entropy loss scaled by a factor of 5.0. The overall training objective was defined as a weighted sum of these two components.

All models were trained for 100 epochs in full-precision (FP32), followed by an additional 20 epochs of quantisation-aware training (QAT) [29]. A batch size of 16 was used for classification and 4 for KWS. The training was conducted on a single NVIDIA A100 GPU. The Adam optimiser [33] was employed with a learning rate of $2 \cdot 10^{-4}$, weight decay of $1 \cdot 10^{-4}$, and a ReduceLROnPlateau scheduler with a reduction factor of 0.5 and patience of 10 epochs. Model checkpoints were selected based on the lowest training loss for the SHD and evaluation loss for the SSC and subsequently evaluated on the test set.

For evaluation, we employed task-specific metrics. In classification, the primary metric was the top-1 accuracy. In KWS, two complementary metrics were used:

- (1) **Top-1 accuracy at maximum confidence** (Acc_K), defined as the classification accuracy at the timestep with the highest predicted confidence.
- (2) **Tolerance-aware top-1 accuracy** ($Acc_{K,\Delta}$), which extends Acc_K by considering predictions correct if the maximum-confidence timestep falls within a tolerance window of ± 1 temporal bin from the ground truth onset.

The hardware architecture of the network was implemented in the SystemVerilog language using Vivado 2022.2, while the processing system was programmed using Vitis 2022.2 in the C++ language. After verifying the compatibility with PyTorch software model via Vivado simulation, it was implemented on a Zynq UltraScale+ ZCU104 FPGA platform with XCZU7EV chip from AMD Xilinx. As we do not use a physical AC sensor for hardware testing, we employ the FPGA’s processing system to read events from an SD card and feed them to the programmable logic according to their timestamps, thereby simulating the temporal sparsity of the data. Based on experiments conducted with reconfigurable logic, we selected a clock frequency of 200 MHz. This choice ensures low latency while avoiding timing issues during system implementation.

4.2 Ablation studies

In this section, we present the results of experiments conducted to evaluate the influence of hyperparameters and selected operations on the proposed architecture. We begin by analysing the impact of the graph generator parameters. Next, we compare the performance and parameter efficiency of different model variants to assess the scalability of the

Table 2. The impact of search radius r_{ch} and *skip step* parameters on top-1 accuracy. The best results, highlighted in **bold**, were obtained for moderate parameters.

r_{ch}	<i>skip step</i>	top-1 acc. float	top-1 acc. quantised	r_{ch}	<i>skip step</i>	top-1 acc. float	top-1 acc. quantised
100	1	90.95 %	-	30	10	85.43 %	84.23 %
100	5	91.37 %	90.10 %	50	10	88.25 %	87.60 %
100	10	92.74 %	92.30 %	200	10	91.23 %	90.05 %
100	15	90.63 %	89.22 %	250	10	90.47 %	89.72 %
100	20	90.05 %	88.91 %	300	10	89.66 %	88.62 %

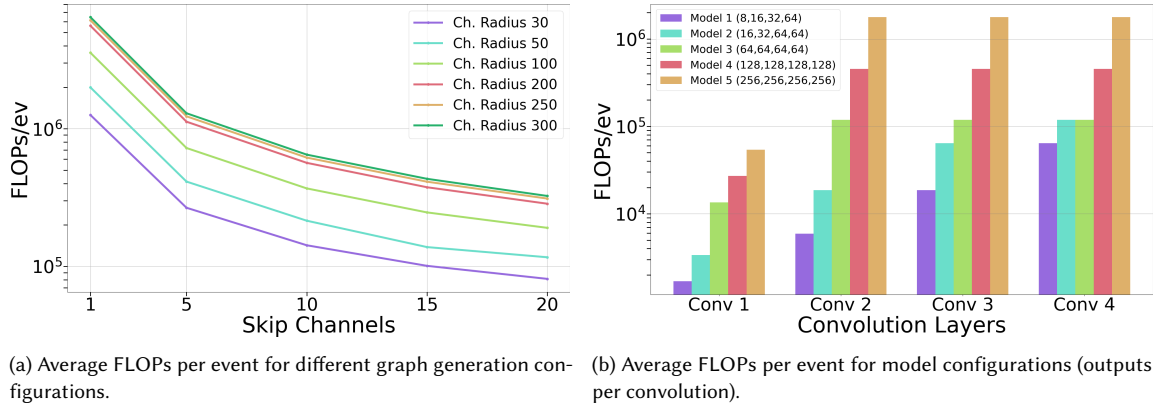
approach. Finally, we evaluate the effect of max, mean, and average operations in graph pooling for both classification and keyword spotting tasks. Unless stated otherwise, the base model was configured with all output channels set to 64, a graph generator with an r_{ch} of 100, a *skip step* of 10, an r_t of 20 ms and using the SHD dataset.

4.2.1 Graph generation configurations. In Table 2 we present the results of our accuracy analysis for the base model as a function of the r_{ch} and *skip step* parameters. The experiment was carried out in two stages. In the first one, we varied the r_{ch} parameter from 30 to 300 while keeping the *skip step* fixed at 10. In the second stage, using the best r_{ch} value identified in the first stage, we varied the *skip step* parameter from 1 to 20. A “-” score indicates configurations excluded from the analysis due to excessively large tensor sizes that could not fit in the GPU memory.

We observed that too few edges – caused by either a high *skip step* or a low r_{ch} – negatively affect the model accuracy. Conversely, an excessively large r_{ch} or too small *skip step* can also degrade classification performance. This is due to the sensitivity of PointNetConv layers to outliers, which become more noticeable with a large number of edges – a consequence of using a max-type aggregation. The best results were achieved with moderate parameter values: an r_{ch} of 100 and a *skip step* of 10, yielding 92.74% accuracy for the floating-point model. Although it is possible that simultaneously increasing both the r_{ch} and the *skip step* might lead to even better performance, the chosen parameters were sufficient for our study.

It is also important to emphasise that the computational cost of graph convolutions is proportional to the number of edges. As illustrated in Figure 7a, the number of floating-point operations (FLOPs) required per event – for all convolutions, averaged across the entire test dataset – is influenced by the *skip step* parameter. This analysis indicates that using connections with a *skip step* of 10 reduces FLOPs by a factor of ten (3.568 vs 0.368 MFLOPs/ev), confirming a linear relationship between computational demands and the number of generated edges. The role of our novel *skip step* method is crucial for reducing the calculation complexity. Note that this is not specific to the context of FPGA implementations.

4.2.2 Model configurations. In this subsection, we examine how varying the dimensions of the convolutional layers affects model performance. As a reference, we used two model configurations described in [52]: small – with all layer dimensions set to 64 and large – with all layer dimensions set to 256. To explore a broader range of options, we study three additional models: one with all layer sizes set to 128, and two variants with increasing layer size. The results, including layer dimensions, total parameter counts, and classification accuracy on both the SHD and SSC datasets, are summarised in Table 3.



(a) Average FLOPs per event for different graph generation configurations. (b) Average FLOPs per event for model configurations (outputs per convolution).

Fig. 7. Model complexity analysis in term of FLOPs. The figures illustrate not only the significant impact of model size on computational complexity, but also the parameters of the graph generator.

Table 3. Layer configurations (number of output features) with number of parameters and top-1 accuracy. Increasing the number of parameters improves classification results, demonstrating the scalability of our approach.

Name	Conv1	Conv2	Conv3	Conv4	FC	Params [k]	SHD top-1 acc. [%]		SSC-11 top-1 acc. [%]		SSC-35 top-1 acc. [%]	
							float	quantised	float	quantised	float	quantised
tiny	8	16	32	64	64	8.6	89.22	88.78	78.93	78.36	66.97	66.31
small	16	32	64	64	64	12.9	90.54	90.98	80.63	80.16	67.49	67.21
base	64	64	64	64	64	18.9	92.74	92.30	81.89	81.45	68.17	67.92
big	128	128	128	128	128	70.5	93.93	93.31	83.11	82.79	69.54	69.36
large	256	256	256	256	256	272.0	94.64	94.45	84.73	84.32	71.02	70.91

The results demonstrate that increasing the number of parameters improves classification accuracy on both datasets, highlighting the scalability of our method. Importantly, compared to the baseline (achieving 90.0% and 94.3% accuracy on SHD for the small and large models), the equivalent models based on our proposed approach (minor differences in parameter number are due to BatchNorm layers) achieve accuracies of 92.74% and 94.63%, respectively.

A similar trend is observed for the SSC dataset. For SSC-35, accuracy increases steadily from 66.97% for the smallest configuration to 71.02% for the largest one, and for SSC-11 it improves from 78.93% to 84.73%. This improvement demonstrates that our method generalises well across tasks, consistently benefiting from higher model capacity. Furthermore, the performance gap between the floating-point and quantised implementations remains small (below 0.3% in most cases), confirming that the proposed solutions not only facilitate efficient hardware implementation but also preserve accuracy after quantisation.

Similar to the number of edges, another key factor influencing model complexity is the dimensionality of event feature vectors processed by the network. To address this, we conducted an analysis of the average number of FLOPs per event for each convolutional layer, depending on its configuration. The results are presented in Figure 7b. They show that the computational complexity of the first convolutional layer increases linearly with its dimension due to the fixed size of input data (13.516 vs 27.032 kFLOPs/ev for Model 3 vs Model 4), while for subsequent layers in models with uniform dimensions, complexity grows quadratically (118.269 vs 452.801 kFLOPs/ev for Conv 2). Consequently, the

Table 4. Comparison of different operations in graph pooling for the SHD dataset:

(a) classification task		(b) KWS task		
Operation	Acc [%]	Operation	Acc _K [%]	Acc _{K,Δ} [%]
max	85.57	max	90.11	87.19
average	92.74	average	89.71	86.62
add	87.81	add	87.32	83.26

total FLOPs for the evaluated models are 0.091, 0.204, 0.368, 1.385, and 5.366 MFLOPs/ev, respectively. These results underline the importance of careful selection of network parameters to optimise memory and computational costs.

4.2.3 Graph pooling. Tables 4a and 4b present a comparison of the applied operators in graph pooling for the classification task and the keyword spotting task. As described in Section 3, in the classification task the aggregation of information from events processed by the feature extraction module was performed over the entire sample (on average 750 ms, up to a maximum of 1 s). In contrast, for the KWS task, the aggregation was performed within shorter time windows of $\Delta t = 10$ ms.

As a result, in the classification task, the average operator achieved the best performance, while the max and add operators yielded results lower by 7 pps and 5 pps, respectively. The max operator, when applied to such a large number of events, proved to be sensitive to outliers. In the case of KWS, splitting the signal into shorter segments reduced the sensitivity to noise, which made the max operator slightly more effective (by 0.4 pps) compared to average. In both tasks, the add operator negatively impacted performance due to the accumulation of large values into a single feature vector.

4.3 Evaluation of the classification model

Since the tasks of classification and keyword spotting, as well as their corresponding network models, differ substantially, we evaluate the proposed method for each task separately. In this section, we present the results obtained with the classification model and compare them against related approaches evaluated on the same datasets.

4.3.1 Comparison with the state-of-the-art. In order to position our work relative to the state-of-the-art, we first compare accuracy and parameter count of our event-graph neural network software model to other event-based AI approaches on the SHD and SSC datasets. Next, we compare our hardware implementation with two FPGA-based works of spiking neural networks, with consideration of power consumption, latency, and resource utilisation.

The results in Table 5 show that our models are among the smallest in the state-of-the-art while retaining competitive accuracy. On the SHD dataset, our base model requires only 18.9k parameters, being surpassed in compactness only by the small model from [52], which inspired our baseline design, and by certain optimised variants of our own network (see Table 3). Despite its small size, this model achieves a test accuracy of 92.31%, which is comparable to the results of [59] and [68], while using 86.5% and over 99% fewer parameters, respectively. Our largest configuration achieves an accuracy of 94.45%, which is outperformed by six competing models. However, two of these [6, 40] require millions of parameters, while two others [4, 58] require more than 400k parameters, compared to only 272k in our case. Notably, the only solution surpassing ours by a clear margin in both size and accuracy is [26], which achieves 95.1% at 200k parameters.

Table 5. Comparison of accuracy and model size on the SHD and SSC datasets for the classification task. The symbol | indicates that only two models are present, while “–” denotes several intermediate values.

Dataset	Author(s)	Method	Recurrent	Hardware	#Params	top-1 acc. [%]	Year
SHD	Cramer et al. [13]	Recurrent SNN	✓	✗	-	83.2	2020
	Yin et al. [66]	Adaptive SRNN	✓	✗	-	90.4	2021
	Yao et al. [65]	TA-SNN	✗	✗	-	91.1	2021
	Yu et al. [68]	STSC-SNN	✗	✗	2.1M	92.4	2022
	Dampfhofer et al. [18]	Cuba-LIF	✓	✗	139k	87.8	2022
	Bittar et al. [6]	Recurrent SNN	✓	✗	3.9M	94.6	2022
	Rossbroich et al. [55]	Convolutional RSNN	✓	✗	209k	83.5	2022
	Nowotny et al. [47]	EventProp-GeNN	✓	✗	-	84.8	2022
	Hammouamri et al. [26]	DCLS-Delays	✗	✗	200k	95.1	2023
	Sun et al. [59]	DL128-SNN-Dloss	✗	✗	140k	92.6	2023
	Rafeldt et al. [52]	Spectro-temporal graph	✗	✗	17.1 217k	90.0 94.3	2024
	D’Agostino et al. [14]	FF SNN with dendritic delays	✗	✗	224 k	87.6	2024
	Malettira et al. [40]	Temporal Skips with delay learning	✗	✗	1.3M	94.7	2024
	Carpeagna et al. [8]	RSNN on FPGA	✓	✓	-	72.9	2024
	Matimizadeh et al. [41]	Fully configurable FPGA SNN	✓	✓	-	87.8	2024
	Schone et al. [58]	Event-SSM	✓	✗	0.4M	95.9	2024
	Baronig et al. [4]	SE-adLIF	✓	✗	450k	95.8	2025
	Sun et al. [60]	PFA SNN	✗	✗	0.2M	96.3	2025
	Huber et al. [28]	S5-RF	✓	✗	214k	91.9	2025
	Ours	Spectro-temporal graph on SoC FPGA	✗	✓	8.6 - 272k	88.8 - 94.5	2025
SSC	Cramer et al. [13]	Recurrent SNN	✓	✗	-	50.9	2020
	Perez-Nieves et al. [51]	Heter. RSNN	✓	✗	-	57.3	2021
	Yin et al. [66]	Adaptive SRNN	✓	✗	-	57.3	2021
	Dampfhofer et al. [18]	SpikGRU	✓	✗	280k	77.0	2022
	Bittar et al. [6]	Recurrent SNN	✓	✗	3.9M	77.4	2022
	Sadovsky et al. [56]	SNN-CNN	✗	✗	-	72.0	2023
	Hammouamri et al. [26]	DCLS-Delays	✓	✗	0.7 - 2.5M	79.8 - 80.7	2023
	Malettira et al. [40]	Temporal Skips with delay learning	✗	✗	1.4M	80.2	2024
	Schone et al. [58]	Event-SSM	✓	✗	0.1 0.6M	85.3 88.4	2024
	Baronig et al. [4]	SE-adLIF	✓	✗	1.6M	80.4	2025
	Sun et al. [60]	PFA SNN	✗	✗	0.1 0.7M	77.4 80.2	2025
	Huber et al. [28]	S5-RF	✓	✗	1.8M	78.8	2025
	Ours - SSC-11	Spectro-temporal graph on SoC FPGA	✗	✓	8.6 - 272k	78.4 - 84.3	2025
	Ours - SSC-35	Spectro-temporal graph on SoC FPGA	✗	✓	8.6 - 272k	66.3 - 70.9	2025

Importantly, our event-graph approach underwent extensive hardware-aware modifications and quantisation, which inevitably constrain the achievable peak accuracy. The high performance achieved under such constraints demonstrates the suitability of graph neural networks for event-data processing.

When extending the evaluation to the SSC dataset, we observe a consistent pattern. Our smallest SSC model achieves 66.3% top-1 accuracy, scaling up to 70.9% for the largest configuration for SSC-35. On the other hand, for SSC-11, our models achieves from 78.4% to 84.3%. While this result falls short of the very best-performing software-only models (e.g. 88.4% by [58] in case of SSC-35), it is important to note that all prior work on SSC remains purely in the software domain. To the best of our knowledge, no hardware implementation of SSC classification has been reported in the literature, highlighting a significant gap in the field. By providing the first hardware-accelerated results on the SSC, we establish an important baseline for future work, showing that efficient event-graph architectures can be deployed under resource and quantisation constraints while still maintaining competitive performance.

4.3.2 Comparison with other hardware implementations. A direct comparison of our hardware implementation with spiking neural network (SNN)-based approaches from the literature is provided in Table 6. For this analysis, we

Table 6. Comparison of different variants of our architecture with state-of-the-art hardware implementations. The values in parentheses take into account the PS part (classification head) – apart from our last model (PL-head), which was fully realised in the programmable logic part of the SoC FPGA. The values marked with “–” were not mentioned in the respective papers. The resource utilisation for [41] was reported only in terms of percentages; thus, the absolute values were estimated based on the maximum resources available on the ZCU104 board.

Model	Device	Logic cells	LUT	FF	BRAM	DSP	Freq. [MHz]	Latency [μs]	Power [W]	Acc. [%]
Matinizadeh [41]	Zynq ZCU104	–	149,760	92,160	75	–	100	–	1.629 ¹	87.80
Carpegna [8]	Zynq Z7-20	18,268	–	–	51	–	100	540	0.43	72.99
Our (base)	Zynq ZCU104	–	81,567	47,699	70	318	200	8.07 (179)	0.99 (3.73)	92.30
Our (tiny)	Zynq ZCU104	–	34,474	23,713	28	106	200	4.01 (175)	0.78 (3.52)	88.78
Our (2VecMuls)	Zynq ZCU104	–	41,925	30,198	70	164	200	15.2 (186)	0.89 (3.63)	92.30
Our (PL-head)	Zynq ZCU104	–	91,630	51,492	84.5	330	200	8.45	1.08	92.12

¹only the “peak power” was reported in the article.

selected the base model – configured with a graph convolution and head feature dimension of 64 – implemented on the Zynq UltraScale+ ZCU104 board. This configuration was chosen as it provides a favourable trade-off between accuracy and resource utilisation, offering relatively high accuracy while maintaining a compact design. In Section 4.3.3, we further report evaluation metrics for alternative model configurations to illustrate the scalability and flexibility of the proposed approach.

The proposed approaches for FPGA-implemented event-audio data classification, can be compared in terms of:

- (1) **Accuracy.** With our approach, we established a new state-of-the-art accuracy for an FPGA solution applied to the SHD benchmark by a considerable 4.5% margin.
- (2) **Utilisation.** The detailed resource utilisation presented in Table 6 demonstrates the applicability of our approach to relatively small embedded SoC FPGA platforms. To achieve a more balanced use of available logic resources compared to [41], we implemented part of the multiplication operations using DSP modules, thereby mitigating potential routing delays. The hardware modules are parametrised such that each multiplication can be flexibly mapped either to DSPs or logic resources. Although graph convolutional neural networks are often criticised for their memory-intensive inference [61] – stemming from the need to store and access features of neighbouring nodes – our optimised memory management, combined with the proposed enhancements to graph generation, resulted in memory utilisation comparable to that of spiking neural network-based systems.
- (3) **Latency.** An important advantage of our solution is its asynchronous event-by-event processing and the intrinsic ability of event-graphs to exploit temporal sparsity for rapid and efficient calculations. However, this makes it difficult to compare it with other solutions in terms of latency. Since each event is processed immediately upon registration and the hardware module does not rely on prior aggregation, we define latency in this study as the time elapsed between the arrival of the last event in the processed sample and the generation of the corresponding prediction. Using this methodology, we measured the per-event latency for graph generation and feature extraction to be 8 μs at a 200 MHz clock frequency, with a throughput of 555 kEPS. After taking into account the PS-PL communication and the determination of the value of classification results by the network’s head in the processing part of the heterogeneous system, we obtain the predicted class 179 μs after the occurrence of the last event. In [8] the reported latency of 0.54 ms assumes the processing of the entire data sample after its encoding in 100 timesteps. Our solution, which requires no prior data aggregation, maintains high throughput and low latency for edge applications by exploiting data’s temporal sparsity.

(4) **Power.** As our system is designed to exploit the inherent sparsity of event data, its dynamic power consumption strongly depends on the amount of activity registered by the AC sensor. To obtain an accurate estimate of average power consumption, we followed the methodology of [41]: we use simulations to extract net toggle rates, which are then supplied to the Vivado Power Analyzer to compute average dynamic power. For this purpose, we generated a representative custom data sample with events occurring every 50 μ s (consistent with an average event rate of 20 kEPS for the SHD dataset). Event frequencies (channels) were selected to create a worst-case scenario in terms of the number of graph edges. The power estimation provided by the Vivado software for the PL part of the system (base model) is 0.99 W (0.396 W dynamic and 0.594 W static). With the PS part included energy usage increases to 3.73 W (3.25 W dynamic and 0.7 W static) for the entire base architecture. While the average power consumption of our system – when relying on the processing system to generate the final prediction – is higher than that reported in [8] and [41], the substantially higher accuracy and smaller latency achieved with our approach justifies this additional cost. Moreover, by integrating the network head directly into the programmable logic, we obtain far more competitive results, as demonstrated in Section 4.3.3.

4.3.3 Hardware module scalability. A key advantage of the proposed method lies in its scalability and flexibility. In this section, we present a series of experiments conducted on the time-series classification model to evaluate modified architectures against the baseline. The resulting metrics are summarised in Table 6.

Evaluation of the tiny model. To demonstrate the scalability of our hardware module, we implemented the tiny configuration, which represents the smallest model described in Table 3. Reducing the output dimensions of the graph convolution modules leads to a substantial decrease in logic, DSP, and memory utilisation. This outcome is expected, as the smaller model requires fewer multiplications and stores fewer features. An additional benefit is a significantly reduced latency, approximately 50% of that observed in the baseline implementation for graph generation and feature extraction. The power consumption estimated for this configuration is also the smallest, as expected (just 0.186 W dynamic, 0.593 W static).

It is noteworthy that the tiny model achieved 0.8% higher accuracy while utilising only 23% of LUTs and 37% of BRAMs compared to [41] – see Table 6.

Decreased number of parallel multiplications. For an additional ablation study we implemented the resource-optimised variant of the base model for decreased number of parallel multiplications (from 4 per convolution to 2) – **2VecMuls model** in Table 6. With this modification, we were able to achieve 49% decrease in both DSP and LUT utilisation and 35% in FFs with a simultaneous increase of latency for a single event (in the PL) to 15.2 μ s (theoretical throughput of 277 kEPS). This experiment confirms that the systems latency and resource utilisation (and thus power consumption) is highly correlated – the choice of the final solution should be based on the requirements of the specific task and the size of the target platform.

Classification head integrated into programmable logic. As indicated in Section 3.2.2, while in the baseline implementation the classification head was developed for the processing system of the heterogenous platform, it is possible to implement entire network pipeline for the programmable logic as end-to-end system. For this purpose, we implemented two MLP layers with ReLU activation, computed using two vector multiplication modules (processing two rows in parallel). With this modification, logic resource utilisation increased by 12%, flip-flops by 8%, BRAMs by 21%, and DSPs by 4%. However, in this configuration, the use of the processing system portion of the heterogeneous device is no longer necessary, resulting in a significant reduction in both latency (time between receiving the last event

Table 7. Results of the floating-point (FP32) and quantised (8-bit) models for the keyword spotting task on the SHD and SSC datasets.

Dataset	#Params	Float		Quantised	
		Acc_K [%]	$Acc_{K,\Delta}$ [%]	Acc_K [%]	$Acc_{K,\Delta}$ [%]
SHD	60.34k	90.11	87.19	88.69	85.91
SSC-11	59.77k	76.21	73.66	73.49	71.30
SSC-35	61.52k	66.80	64.45	64.74	63.12

and generating the prediction is $8.45 \mu\text{s}$) and power consumption (estimated at 1.08 W, comprising 0.486 W dynamic and 0.595 W static power). As the weights in the network’s head have been quantised for hardware implementation, the network’s accuracy is 0.18 pps smaller.

The particular configuration of the proposed hardware system can be chosen based on specific application’s requirements and resource availability on the target platform.

4.4 Evaluation of the KWS model

In this section, we present the evaluation of an end-to-end implementation of the KWS module on the programmable logic of a heterogeneous FPGA platform, specifically the Zynq UltraScale+ ZCU104 board. For this experiment, all layers (including the output head) were quantised to 8-bit integer values. The output feature size of each graph convolution layer, as well as the STEM and GRU modules, was fixed at 72 in order to efficiently utilise the BRAM blocks and their 36-bit word size.

The hardware module was first verified through Vivado simulation to ensure compatibility with the software model and subsequently implemented on the target platform. For the purposes of this evaluation, the clock frequency was set to 200 MHz. It should be noted, however, that the KWS model design does not restrict the user from selecting lower clock frequencies, thereby enabling reduced power consumption at the cost of increased latency.

The results of software-based model training and corresponding model sizes are presented in Table 7. The average model size is approximately 60k parameters, with minor variations due to the different numbers of output classes. On the SHD dataset, accuracy decreases from 92.74% for the base classification task to 90.11% in the KWS task (FP32), reflecting the higher complexity of the latter, where classification relies on the maximum confidence score across the entire sample. Furthermore, when comparing top-1 accuracy with keyword detection at the generated offset, the accuracy is approximately 87.19%, which is a satisfactory outcome for such a challenging task.

Similarly, for the SSC dataset, both variants (11 and 35 classes) demonstrate that the difference between Acc_K and $Acc_{K,\Delta}$ is around 2.5%. For all datasets, the models successfully detect the end of the keyword (within a $\pm 1\Delta t$ offset) in more than 95% of cases. Additionally, reducing the number of classes in SSC increases accuracy by approximately 10%.

The evaluation metrics of the KWS model implemented in hardware are presented in Table 8. Our method achieves high accuracy (see Table 7 – quantised results) with a low latency of only $10.53 \mu\text{s}$ for end-to-end KWS task with prediction generated every 10 ms. Latency is measured as the time between receiving the last event in a time window and generating the prediction. The low resource utilisation further enables deployment on relatively small, embedded FPGA platforms. Moreover, this architecture can be applied to continuous event streams, as the recurrent head naturally supports such processing.

Table 8. Resource utilisation, latency and power consumption for KWS model as described in Section 4.4. We report the metrics for entire architecture as well as graph generation + feature extraction + pooling (FE + pool) and GRU head separately.

	FE + pool	GRU head	Total
LUT	99,940	25,190	125,130
FF	55,182	27,190	82,372
BRAM	58.5	17	75.5
DSP	108	32	140
Latency [μs]	8.48	2.05	10.53
Average power [W]	1.03	0.15	1.18

Average power consumption was estimated using the Vivado Power Analyzer, based on net toggle rates extracted from a representative data sample. The event rate was aligned with the average of 20 kEPS established for the SHD dataset, while frequencies were chosen to represent a worst-case scenario in terms of the number of graph edges. The achieved average consumption of 1.184 W (0.588 dynamic, 0.595 static) underscores the applicability of our method to energy-constrained use cases, such as Internet-of-Things edge devices. As indicated in Table 8, while the network head consumes a considerable portion of resources (20% of all LUTs and 33% of all FFs used in the system), it accounts for only 13% of the total power consumption. This is due to its activity for just 2.06 μ s every 10 ms, being triggered only after the pooling module.

To the best of our knowledge, this work represents the first hardware implementation of a KWS system that processes audio in the event-driven domain. As such, it can serve as a benchmark for future research.

4.5 Comparison with embedded GPU

To evaluate the temporal and energy efficiency of the proposed method in comparison with alternative embedded platforms, a reference implementation was developed on the Jetson Orin NX platform. This system is equipped with an ARM Cortex-A78 processor and an NVIDIA Ampere GPU. To ensure comparability with the FPGA configuration, a graph generator was implemented in C++ and executed on a single CPU core in an event-by-event manner. The generated graph was subsequently processed by the model on both the GPU and CPU at two power modes: 10 W and MAXN.

In the Jetson setup, three latency-inducing stages can be distinguished: (i) per-event graph generation, (ii) parsing the generated graph into a Torch tensor, and (iii) model inference. In contrast, on the FPGA platform, the graph generator, feature extractor and graph pooling operate in an event-by-event manner, after which only the head processes the pooled graph outputs. For each task, latency is measured after the arrival of the last event within the temporal window (1 s for classification and 10 ms for keyword spotting).

Figure 8 reports the latency of each stage (logarithmic scale on the y-axis). Since graph generation and parsing are executed on the CPU, their values are comparable in both CPU and GPU-based configurations. At the 10 W power level, graph generation requires on average 1 μ s per event, whereas at MAXN this time is reduced to 0.42 μ s. Parsing the graph into a tensor takes 3.69 ms and 1.71 ms, respectively. Considering only the fastest Jetson configuration (GPU-MAXN), forward propagation for the tiny/base/KWS models requires 71.51 ms, 107.47 ms, and 96.16 ms, respectively. By contrast, our FPGA implementation achieves 4.01 μ s, 8.07 μ s, and 8.48 μ s per event for graph generation and feature extraction,

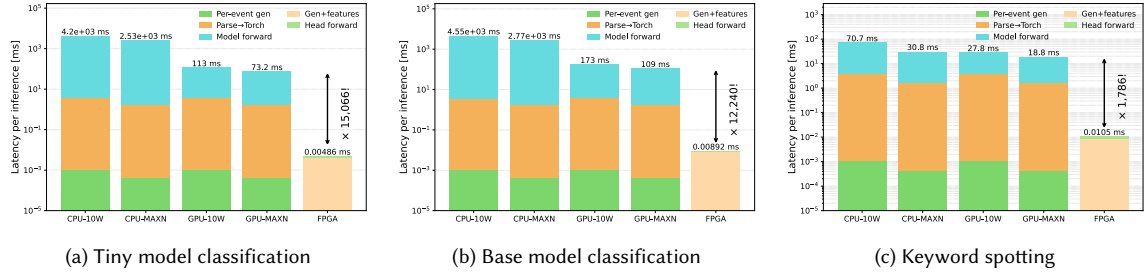


Fig. 8. Latency comparison of tiny, base, and keyword spotting models on Jetson Orin NX (CPU/GPU) and ZCU104 FPGA.

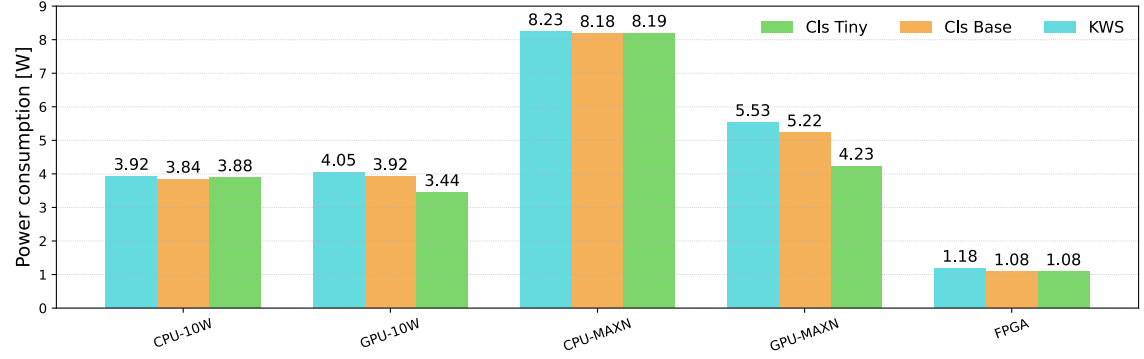


Fig. 9. Power consumption of tiny, base, and keyword spotting models on Jetson Orin NX (CPU/GPU) and ZCU104 FPGA.

as well as $0.85 \mu\text{s}$ and $2.05 \mu\text{s}$ for classification and keyword spotting heads. These results correspond to speed-ups of more than $15,000\times$, $12,000\times$, and $1,700\times$ compared to Jetson.

Figure 9 presents the power consumption results for each configuration. The measurements demonstrate that our hardware implementation on the ZCU104 consumes up to $4\times$ less power than the GPU-MAXN configuration and up to $8\times$ less than the CPU-MAXN, highlighting that our solution surpasses Jetson in both latency and power efficiency.

5 Summary

In this work we present the first hardware implementation of an event-graph neural network for time-series audio classification and keyword spotting tasks. As our approach exploits the inherent sparsity of event-data to reduce the computational complexity and latency, it is highly promising for near-sensor AI processing at the edge. We proposed adaptations and optimisations permitting an event-graph to be implemented efficiently in a SoC FPGA. In particular, we presented the novel *skip step* graph generation method with simplified and computationally efficient features.

In spite of this, for time-series classification our quantised hardware-aware event-graph model achieved a test accuracy extremely close to floating-point precision software models from the state-of-the-art while requiring almost two orders of magnitude fewer parameters. Crucially, our method outperformed all previous FPGA implementations of hardware-aware spiking neural networks on the same classification benchmark achieving improvements of 4.5% and 19.3% in accuracy. Relative to these works, the utilisation of FPGA resources and the latency were also reduced. Our smallest model (tiny) achieves accuracy comparable to previous hardware state-of-the-art implementations while using

only 23% of the logic and 37% of the memory resources. Moreover, our end-to-end implementation – which includes graph generation, feature extraction, and the classification head – supports real-time processing with a latency of just 8.45 μ s and an average power consumption of 1.08 W, achieving 4.32 pps higher accuracy with a relatively similar model size compared to [41].

We also proposed a separate architecture for a keyword spotting task, that utilises graph convolutional neural networks for feature extraction and a recurrent head for final prediction. Our end-to-end hardware implementation enables real-time KWS on continuous stream with prediction generated every 10 ms with the latency of just 10.53 μ s and average power consumption estimated at 1.18 W.

To ensure comparability, we evaluated our model on open-source datasets: SHD, SSC-11, and SSC-35, achieving tolerance-aware top-1 accuracy of 85.91%, 71.30%, and 63.12%, respectively. Additionally, the model attained a word-end detection accuracy exceeding 95%, thereby enabling other researchers to directly assess and extend our results.

To the best of our knowledge, there are no prior works addressing keyword spotting on these datasets; thus, our results establish a baseline for this task. Nevertheless, several strategies could further improve performance, such as data augmentation through random noise injection or random temporal offsets.

Additionally, we conducted a comparison of our solution with the implementation on the Jetson Orin NX, which demonstrated that our hardware architecture achieves latency reductions of approximately 15,000 \times , 12,000 \times , and 1,700 \times for the tiny, base, and keyword spotting models, respectively, while reducing energy consumption by more than 4 \times compared to the GPU and 8 \times compared to the CPU.

We have confirmed that the hardware implementation of graph neural networks applied to event data from artificial cochlea sensors is both highly efficient and capable of achieving superior task accuracy and latency compared to spiking neural network alternatives. In future work, we intend to integrate real AC sensor with our FPGA implementation of the graph neural network for a fully end-to-end system. We also plan to implement NAS sensor in FPGA's resources and connect it with our hardware module to allow a comparison of these two approaches. Finally, we intend to deploy the complete system on an ASIC to further reduce power consumption.

6 Acknowledgments

This work was supported by The Horizon Europe (dAIedge, grant 101120726), the “Excellence initiative – research university” programme for the AGH University of Krakow, the Polish National Science Centre projects 2024/53/N/ST6/04254 and 2024/53/N/ST6/04331 and Polish high-performance computing infrastructure PLGrid (HPC Center: ACK Cyfronet AGH – grant no. PLG/2023/016897).

References

- [1] Harsh Ahlawat, Naveen Aggarwal, and Deepthi Gupta. 2025. Automatic Speech Recognition: A survey of deep learning techniques and approaches. *International Journal of Cognitive Computing in Engineering* 6 (2025), 201–237. [doi:10.1016/j.ijcce.2024.12.007](https://doi.org/10.1016/j.ijcce.2024.12.007)
- [2] Firas Al-Ali, Thilina Doremure Gamage, Hewa WTS Nanayakkara, Farhad Mehdipour, and Sayan Kumar Ray. 2020. Novel Casestudy and Benchmarking of AlexNet for Edge AI: From CPU and GPU to FPGA. In *2020 IEEE Canadian Conference on Electrical and Computer Engineering (CCECE)*. 1–4. [doi:10.1109/CCECE47787.2020.9255739](https://doi.org/10.1109/CCECE47787.2020.9255739)
- [3] Yasir Al-Ameri, Ming Nguyen, and Tomi Westerlund. 2024. FPGA-Based Hardware Acceleration for Deep Learning in Mobile Robotics. In *2024 IEEE Nordic Circuits and Systems Conference (NorCAS)*. 1–7. [doi:10.1109/NorCAS64408.2024.10752450](https://doi.org/10.1109/NorCAS64408.2024.10752450)
- [4] Maximilian Baronig, Romain Ferrand, Silvester Sabathiel, and Robert Legenstein. 2025. Advancing spatio-temporal processing through adaptation in spiking neural networks. *Nature Communications* 16, 1 (01 Jul 2025), 5776. [doi:10.1038/s41467-025-60878-z](https://doi.org/10.1038/s41467-025-60878-z)
- [5] Arindam Basu, Lei Deng, Charlotte Frenkel, and Xueyong Zhang. 2022. Spiking neural network integrated circuits: A review of trends and future directions. In *2022 IEEE Custom Integrated Circuits Conference (CICC)*. IEEE, 1–8. [doi:10.1109/CICC53496.2022.9772783](https://doi.org/10.1109/CICC53496.2022.9772783)

- [6] Alexandre Bittar and Philip N. Garner. 2022. A surrogate gradient spiking baseline for speech command recognition. *Frontiers in Neuroscience* 16 (2022). [doi:10.3389/fnins.2022.865897](https://doi.org/10.3389/fnins.2022.865897)
- [7] Peter Blouw and Chris Eliasmith. 2020. Event-Driven Signal Processing with Neuromorphic Computing Systems. In *ICASSP 2020 - 2020 IEEE International Conference on Acoustics, Speech and Signal Processing (ICASSP)*. 8534–8538. [doi:10.1109/ICASSP40776.2020.9053043](https://doi.org/10.1109/ICASSP40776.2020.9053043)
- [8] Alessio Carpegna, Alessandro Savino, and Stefano Di Carlo. 2024. Spiker+: a framework for the generation of efficient Spiking Neural Networks FPGA accelerators for inference at the edge. *IEEE Transactions on Emerging Topics in Computing* 01 (Dec. 2024), 1–15. [doi:10.1109/TETC.2024.3511676](https://doi.org/10.1109/TETC.2024.3511676)
- [9] Enea Ceolini, Jithendar Anumula, Stefan Braun, and Shih-Chii Liu. 2019. Event-driven Pipeline for Low-latency Low-compute Keyword Spotting and Speaker Verification System. In *ICASSP 2019 - 2019 IEEE International Conference on Acoustics, Speech and Signal Processing (ICASSP)*. 7953–7957. [doi:10.1109/ICASSP.2019.8683669](https://doi.org/10.1109/ICASSP.2019.8683669)
- [10] R. Qi Charles, Hao Su, Mo Kaichun, and Leonidas J. Guibas. 2017. PointNet: Deep Learning on Point Sets for 3D Classification and Segmentation. In *2017 IEEE Conference on Computer Vision and Pattern Recognition (CVPR)*. 77–85. [doi:10.1109/CVPR.2017.16](https://doi.org/10.1109/CVPR.2017.16)
- [11] Guoguo Chen, Carolina Parada, and Georg Heigold. 2014. Small-footprint keyword spotting using deep neural networks. In *2014 IEEE International Conference on Acoustics, Speech and Signal Processing (ICASSP)*. 4087–4091. [doi:10.1109/ICASSP.2014.6854370](https://doi.org/10.1109/ICASSP.2014.6854370)
- [12] Kyunghyun Cho, Bart van Merriënboer, Dzmitry Bahdanau, and Yoshua Bengio. 2014. On the Properties of Neural Machine Translation: Encoder-Decoder Approaches. arXiv:1409.1259 [cs.CL]
- [13] Benjamin Cramer, Yannik Stradmann, Johannes Schemmel, and Friedemann Zenke. 2022. The Heidelberg Spiking Data Sets for the Systematic Evaluation of Spiking Neural Networks. *IEEE Transactions on Neural Networks and Learning Systems* 33, 7 (2022), 2744–2757. [doi:10.1109/TNNLS.2020.3044364](https://doi.org/10.1109/TNNLS.2020.3044364)
- [14] Simone D'Agostino, Filippo Moro, Tristan Torchet, Yiğit Demirag, Laurent Grenouillet, Giacomo Indiveri, Elisa Vianello, and Melika Payvand. 2024. DenRAM: Neuromorphic Dendritic Architecture with RRAM for Efficient Temporal Processing with Delays. *Nature Communications* 15, 3446 (2024). <https://doi.org/10.1038/s41467-024-47764-w>
- [15] Thomas Dalgaty, Thomas Mesquida, Damien Joubert, Amos Sironi, Cyrille Soubeyrat, Pascal Vivet, and Christoph Posch. 2023. The CNN vs. SNN Event-camera Dichotomy and Perspectives For Event-Graph Neural Networks. In *2023 Design, Automation & Test in Europe Conference & Exhibition (DATE)*. IEEE, 1–6. [doi:10.23919/DATE56975.2023.10137023](https://doi.org/10.23919/DATE56975.2023.10137023)
- [16] Thomas Dalgaty, Thomas Mesquida, Damien Joubert, Amos Sironi, Pascal Vivet, and Christoph Posch. 2023. HUGNet: Hemi-Spherical Update Graph Neural Network Applied to Low-Latency Event-Based Optical Flow. In *Proceedings of the IEEE/CVF Conference on Computer Vision and Pattern Recognition (CVPR) Workshops*. 3952–3961. [doi:10.1109/CVPRW59228.2023.00411](https://doi.org/10.1109/CVPRW59228.2023.00411)
- [17] Thomas Dalgaty, Filippo Moro, Yiğit Demirag, Alessio De Pra, Giacomo Indiveri, Elisa Vianello, and Melika Payvand. 2024. Mosaic: in-memory computing and routing for small-world spike-based neuromorphic systems. *Nature Communications* 15, 1 (2024), 142. [doi:10.1038/s41467-023-44365-x](https://doi.org/10.1038/s41467-023-44365-x)
- [18] Manon Dampfhofer, Thomas Mesquida, Alexandre Valentian, and Lorena Anghel. 2022. Investigating Current-Based and Gating Approaches for Accurate and Energy-Efficient Spiking Recurrent Neural Networks. In *Artificial Neural Networks and Machine Learning – ICANN 2022*, Elias Pimenidis, Plamen Angelov, Chrisina Jayne, Antonios Papaleonidas, and Mehmet Aydin (Eds.). Springer Nature Switzerland, Cham, 359–370. [doi:10.1007/978-3-031-15934-3_30](https://doi.org/10.1007/978-3-031-15934-3_30)
- [19] Manon Dampfhofer, Thomas Mesquida, Alexandre Valentian, and Lorena Anghel. 2023. Are SNNs Really More Energy-Efficient Than ANNs? an In-Depth Hardware-Aware Study. *IEEE Transactions on Emerging Topics in Computational Intelligence* 7, 3 (2023), 731–741. [doi:10.1109/TETCI2022.3214509](https://doi.org/10.1109/TETCI2022.3214509)
- [20] S. Davis and P. Mermelstein. 1980. Comparison of parametric representations for monosyllabic word recognition in continuously spoken sentences. *IEEE Transactions on Acoustics, Speech, and Signal Processing* 28, 4 (1980), 357–366. [doi:10.1109/TASSP.1980.1116340](https://doi.org/10.1109/TASSP.1980.1116340)
- [21] John P DiMarco. 2003. Implantable cardioverter-defibrillators. *New England Journal of Medicine* 349, 19 (2003), 1836–1847. [doi:10.1056/NEJMra035432](https://doi.org/10.1056/NEJMra035432)
- [22] Juan P. Dominguez-Morales, Qian Liu, Robert James, Daniel Gutierrez-Galan, Angel Jimenez-Fernandez, Simon Davidson, and Steve Furber. 2018. Deep Spiking Neural Network model for time-variant signals classification: a real-time speech recognition approach. In *2018 International Joint Conference on Neural Networks (IJCNN)*. 1–8. [doi:10.1109/IJCNN.2018.8489381](https://doi.org/10.1109/IJCNN.2018.8489381)
- [23] William Falcon and The PyTorch Lightning team. 2019. *PyTorch Lightning*. [doi:10.5281/zenodo.3828935](https://doi.org/10.5281/zenodo.3828935)
- [24] Guillermo Gallego, Tobi Delbrück, Garrick Orchard, Chiara Bartolozzi, Brian Taba, Andrea Censi, Stefan Leutenegger, Andrew J Davison, Jörg Conradt, Kostas Daniilidis, et al. 2020. Event-based vision: A survey. *IEEE Transactions on Pattern Analysis and Machine Intelligence* 44, 1 (2020), 154–180. [doi:10.1109/TPAMI.2020.3008413](https://doi.org/10.1109/TPAMI.2020.3008413)
- [25] Kaiyuan Guo, Shulin Zeng, Jincheng Yu, Yu Wang, and Huazhong Yang. 2019. [DL] A Survey of FPGA-based Neural Network Inference Accelerators. *ACM Trans. Reconfigurable Technol. Syst.* 12, 1, Article 2 (March 2019), 26 pages. [doi:10.1145/3289185](https://doi.org/10.1145/3289185)
- [26] Ilyass Hammouamri, Ismail Khalfaoui-Hassani, and Timothée Masquelier. 2023. Learning Delays in Spiking Neural Networks using Dilated Convolutions with Learnable Spacings. arXiv:2306.17670 [cs.NE] <https://arxiv.org/abs/2306.17670>
- [27] Sepp Hochreiter and Jürgen Schmidhuber. 1997. Long Short-Term Memory. *Neural Computation* 9, 8 (1997), 1735–1780. [doi:10.1162/neco.1997.9.8.1735](https://doi.org/10.1162/neco.1997.9.8.1735)
- [28] Thomas E. Huber, Jules Lecomte, Borislav Polovnikov, and Axel von Arnim. 2025. Scaling Up Resonate-and-Fire Networks for Fast Deep Learning. In *Computer Vision – ECCV 2024 Workshops*, Alessio Del Bue, Cristian Canton, Jordi Pont-Tuset, and Tatiana Tommasi (Eds.). Springer Nature Switzerland, Cham, 241–258. [doi:10.1007/978-3-031-92460-6_15](https://doi.org/10.1007/978-3-031-92460-6_15)
- [29] Benoit Jacob, Skirmantas Kligys, Bo Chen, Menglong Zhu, Matthew Tang, Andrew Howard, Hartwig Adam, and Dmitry Kalenichenko. 2018. Quantization and training of neural networks for efficient integer-arithmetic-only inference. In *Proceedings of the IEEE conference on computer vision*

and pattern recognition. 2704–2713. doi:[10.1109/CVPR.2018.00286](https://doi.org/10.1109/CVPR.2018.00286)

[30] Kamil Jeziorek, Andrea Pinna, and Tomasz Kryjak. 2023. Memory-efficient graph convolutional networks for object classification and detection with event cameras. In *2023 Signal Processing: Algorithms, Architectures, Arrangements, and Applications (SPA)*. IEEE, 160–165. doi:[10.23919/SPA59660.2023.10274464](https://doi.org/10.23919/SPA59660.2023.10274464)

[31] Kamil Jeziorek, Piotr Wzorek, Krzysztof Blachut, Andrea Pinna, and Tomasz Kryjak. 2024. Embedded Graph Convolutional Networks for Real-Time Event Data Processing on SoC FPGAs. arXiv:2406.07318 [cs.CV] <https://arxiv.org/abs/2406.07318>

[32] Byeonggeun Kim, Simyung Chang, Jinkyu Lee, and Dooyong Sung. 2021. Broadcasted Residual Learning for Efficient Keyword Spotting. In *Proc. Interspeech 2021*. 4538–4542. doi:[10.21437/Interspeech.2021-383](https://doi.org/10.21437/Interspeech.2021-383)

[33] Diederik P Kingma. 2014. Adam: A method for stochastic optimization. *arXiv preprint arXiv:1412.6980* (2014).

[34] Adithya Krishna, H Shankaranarayanan, Hitesh Pavan Oleti, Anand Chauhan, André van Schaik, Mahesh Mehendale, and Chetan Singh Thakur. 2023. TinyML Acoustic Classification using RAMAN Accelerator and Neuromorphic Cochlea. In *2023 IEEE Asia Pacific Conference On Postgraduate Research In Microelectronics And Electronics (PRIMEAsia)*. 44–45. doi:[10.1109/PRIMEAsia60757.2023.00022](https://doi.org/10.1109/PRIMEAsia60757.2023.00022)

[35] Tomasz Kryjak. 2024. Event-Based Vision on FPGAs-a Survey. In *2024 27th Euromicro Conference on Digital System Design (DSD)*. IEEE, 541–550. doi:[10.1109/DSD64264.2024.00078](https://doi.org/10.1109/DSD64264.2024.00078)

[36] Yijin Li, Han Zhou, Bangbang Yang, Ye Zhang, Zhaopeng Cui, Hujun Bao, and Guofeng Zhang. 2021. Graph-based asynchronous event processing for rapid object recognition. In *Proceedings of the IEEE/CVF International Conference on Computer Vision*. 934–943. doi:[10.1109/ICCV48922.2021.00097](https://doi.org/10.1109/ICCV48922.2021.00097)

[37] Bryan Lim and Stefan Zohren. 2021. Time-series forecasting with deep learning: a survey. *Philosophical Transactions of the Royal Society A* 379, 2194 (2021), 20200209. doi:[10.1098/rsta.2020.0209](https://doi.org/10.1098/rsta.2020.0209)

[38] Shih-Chii Liu, Andre van Schaik, Bradley A Minch, and Tobi Delbrück. 2013. Asynchronous Binaural Spatial Audition Sensor With $2 \times 64 \times 4$ Channel Output. *IEEE Transactions on Biomedical Circuits and Systems* 8, 4 (2013), 453–464. doi:[10.1109/TBCAS.2013.2281834](https://doi.org/10.1109/TBCAS.2013.2281834)

[39] Iván López-Espejo, Zheng-Hua Tan, John H. L. Hansen, and Jesper Jensen. 2022. Deep Spoken Keyword Spotting: An Overview. *IEEE Access* 10 (2022), 4169–4199. doi:[10.1109/ACCESS.2021.3139508](https://doi.org/10.1109/ACCESS.2021.3139508)

[40] Prajna G. Malettira, Shubham Negi, Wachirawit Ponghiran, and Kaushik Roy. 2024. TSkip: Efficiency Through Explicit Temporal Delay Connections in Spiking Neural Networks. arXiv:2411.16711 [cs.NE] <https://arxiv.org/abs/2411.16711>

[41] Shadi Matinizadeh, Noah Pacik-Nelson, Ioannis Polykretis, Krupa Tishbi, Suman Kumar, M. L. Varshika, Arghavan Mohammadhassani, Abhishek Mishra, Nagarajan Kandasamy, James Shackleford, Eric Gallo, and Anup Das. 2024. A Fully-Configurable Open-Source Software-Defined Digital Quantized Spiking Neural Core Architecture. arXiv:2404.02248 [cs.AR] <https://arxiv.org/abs/2404.02248>

[42] Thomas Mesquida, Manon Dampfhofer, Thomas Dalgaty, Pascal Vivet, Amos Sironi, and Christoph Posch. 2023. G2N2: Lightweight event stream classification with GRU graph neural networks. In <https://proceedings.bmvc2023.org/> (<https://proceedings.bmvc2023.org/>). Aberdeen, United Kingdom, 660. <https://cea.hal.science/cea-04321175>

[43] Ali Mostafa, Emmanuel Hardy, and Franck Badets. 2024. 17.8 0.4 V 988nW Time-Domain Audio Feature Extraction for Keyword Spotting Using Injection-Locked Oscillators. In *2024 IEEE International Solid-State Circuits Conference (ISSCC)*, Vol. 67. IEEE, 328–330. doi:[10.1109/ISSCC49657.2024.10454389](https://doi.org/10.1109/ISSCC49657.2024.10454389)

[44] Soufiane Mourrane, Benoit Larras, Sylvain Clerc, Andreia Cathelin, and Antoine Frappé. 2023. Low-Power Event-Driven Spectrogram Extractor for Multiple Keyword Spotting: A proof of concept. In *2023 21st IEEE Interregional NEWCAS Conference (NEWCAS)*. 1–5. doi:[10.1109/NEWCAS57931.2023.10198120](https://doi.org/10.1109/NEWCAS57931.2023.10198120)

[45] Hiroshi Nakano, Krzysztof Blachut, Kamil Jeziorek, Piotr Wzorek, Manon Dampfhofer, Thomas Mesquida, Hiroaki Nishi, Tomasz Kryjak, and Thomas Dalgaty. 2025. Hardware-Accelerated Event-Graph Neural Networks for Low-Latency Time-Series Classification on SoC FPGA. In *Applied Reconfigurable Computing: Architectures, Tools, and Applications*, Roberto Giorgi, Mirjana Stojilović, Dirk Stroobandt, Piedad Brox Jiménez, and Ángel Barriga Barros (Eds.). Springer Nature Switzerland, Cham, 51–68. doi:[10.1007/978-3-031-87995-1_4](https://doi.org/10.1007/978-3-031-87995-1_4)

[46] Wei Soon Ng, Wang Ling Goh, and Yuan Gao. 2024. High Accuracy and Low Latency Mixed Precision Neural Network Acceleration for TinyML Applications on Resource-Constrained FPGAs. In *2024 IEEE International Symposium on Circuits and Systems (ISCAS)*. 1–5. doi:[10.1109/ISCAS58744.2024.10558440](https://doi.org/10.1109/ISCAS58744.2024.10558440)

[47] Thomas Nowotny, James P Turner, and James C Knight. 2025. Loss shaping enhances exact gradient learning with Eventprop in spiking neural networks. *Neuromorphic Computing and Engineering* 5, 1 (jan 2025), 014001. doi:[10.1088/2634-4386/ada852](https://doi.org/10.1088/2634-4386/ada852)

[48] Thomas Ortner, Lorenzo Pes, Joris Gentinetta, Charlotte Frenkel, and Angeliki Pantazi. 2023. Online spatio-temporal learning with target projection. In *2023 IEEE 5th International Conference on Artificial Intelligence Circuits and Systems (AICAS)*. IEEE, 1–5. doi:[10.1109/AICAS57966.2023.10168623](https://doi.org/10.1109/AICAS57966.2023.10168623)

[49] Adam Paszke, Sam Gross, Soumith Chintala, Gregory Chanan, Edward Yang, Zachary DeVito, Zeming Lin, Alban Desmaison, Luca Antiga, and Adam Lerer. 2017. Automatic differentiation in pytorch. (2017).

[50] Bruno U. Pedroni, Sadique Sheikh, Hesham Mostafa, Somnath Paul, Charles Augustine, and Gert Cauwenberghs. 2018. Small-footprint Spiking Neural Networks for Power-efficient Keyword Spotting. In *2018 IEEE Biomedical Circuits and Systems Conference (BioCAS)*. 1–4. doi:[10.1109/BIOCAS.2018.8584832](https://doi.org/10.1109/BIOCAS.2018.8584832)

[51] Nicolas Perez-Nieves, Vincent C. H. Leung, Pier Luigi Dragotti, and Dan F. M. Goodman. 2021. Neural heterogeneity promotes robust learning. *Nature Communications* 12, 1 (04 Oct 2021), 5791. doi:[10.1038/s41467-021-26022-3](https://doi.org/10.1038/s41467-021-26022-3)

[52] Lars Rafeldt, Thomas Mesquida, Hiroshi Nakano, Manon Dampfhofer, Filippo Moro, Pascal Vivet, Melika Payvand, and Thomas Dalgaty. 2025. Event-based Audio Prediction with Spectro-Temporal Event-Graphs. In *2025 IEEE International Symposium on Circuits and Systems (ISCAS)*. 1–5.

[doi:10.1109/ISCAS56072.2025.11043865](https://doi.org/10.1109/ISCAS56072.2025.11043865)

[53] Lei Ren, Zidi Jia, Yuanjun Laili, and Di Huang. 2023. Deep learning for time-series prediction in IIoT: progress, challenges, and prospects. *IEEE Transactions on Neural Networks and Learning Systems* (2023). [doi:10.1109/TNNLS.2023.3291371](https://doi.org/10.1109/TNNLS.2023.3291371)

[54] J.R. Rohlícek, W. Russell, S. Roukos, and H. Gish. 1989. Continuous hidden Markov modeling for speaker-independent word spotting. In *International Conference on Acoustics, Speech, and Signal Processing*, 627–630 vol.1. [doi:10.1109/ICASSP.1989.266505](https://doi.org/10.1109/ICASSP.1989.266505)

[55] Julian Rossbroich, Julia Gygax, and Friedemann Zenke. 2022. Fluctuation-driven initialization for spiking neural network training. *Neuromorphic Computing and Engineering* 2, 4 (Dec. 2022), 044016. [doi:10.1088/2634-4386/ac97bb](https://doi.org/10.1088/2634-4386/ac97bb)

[56] Erik Sadovsky, Maros Jakubec, and Roman Jarina. 2023. Speech Command Recognition Based on Convolutional Spiking Neural Networks. In *2023 33rd International Conference Radioelektronika (RADIOELEKTRONIKA)*. 1–5. [doi:10.1109/RADIOELEKTRONIKA57919.2023.10109082](https://doi.org/10.1109/RADIOELEKTRONIKA57919.2023.10109082)

[57] Syahril Ramadhan Saufi, Zair Asrar Bin Ahmad, Mohd Salman Leong, and Meng Hee Lim. 2020. Gearbox fault diagnosis using a deep learning model with limited data sample. *IEEE Transactions on Industrial Informatics* 16, 10 (2020), 6263–6271. [doi:10.1109/TII.2020.2967822](https://doi.org/10.1109/TII.2020.2967822)

[58] Mark Schöne, Neeraj Mohan Sushma, Jingyue Zhuge, Christian Mayr, Anand Subramoney, and David Kappel. 2024. Scalable Event-by-Event Processing of Neuromorphic Sensory Signals with Deep State-Space Models. In *2024 International Conference on Neuromorphic Systems (ICONS)*. 124–131. [doi:10.1109/ICONS62911.2024.00026](https://doi.org/10.1109/ICONS62911.2024.00026)

[59] Pengfei Sun, Yansong Chua, Paul Devos, and Dick Botteldooren. 2023. Learnable axonal delay in spiking neural networks improves spoken word recognition. *Frontiers in Neuroscience* 17 (2023). [doi:10.3389/fnins.2023.1275944](https://doi.org/10.3389/fnins.2023.1275944)

[60] Pengfei Sun, Jibin Wu, Paul Devos, and Dick Botteldooren. 2025. Towards parameter-free attentional spiking neural networks. *Neural Networks* 185 (2025), 107154. [doi:10.1016/j.neunet.2025.107154](https://doi.org/10.1016/j.neunet.2025.107154)

[61] Zhaokang Wang, Yunpan Wang, Chunfeng Yuan, Rong Gu, and Yihua Huang. 2021. Empirical analysis of performance bottlenecks in graph neural network training and inference with GPUs. *Neurocomputing* 446 (2021), 165–191.

[62] Pete Warden. 2018. Speech Commands: A Dataset for Limited-Vocabulary Speech Recognition. arXiv:1804.03209 [cs.CL] <https://arxiv.org/abs/1804.03209>

[63] Ying Xu, Samalika Perera, Yeshwanth Bethi, Saeed Afshar, and André van Schaik. 2023. Event-driven spectrotemporal feature extraction and classification using a silicon cochlea model. *Frontiers in Neuroscience* 17 (2023), 1125210. [doi:10.3389/fnins.2023.1125210](https://doi.org/10.3389/fnins.2023.1125210)

[64] Yufeng Yang, Adrian Kneip, and Charlotte Frenkel. 2025. EvGNN: An Event-Driven Graph Neural Network Accelerator for Edge Vision. *IEEE Transactions on Circuits and Systems for Artificial Intelligence* 2, 1 (2025), 37–50. [doi:10.1109/TCASAI.2024.3520905](https://doi.org/10.1109/TCASAI.2024.3520905)

[65] Man Yao, Huanhuan Gao, Guangshe Zhao, Dingheng Wang, Yihan Lin, Zhaoxu Yang, and Guoqi Li. 2021. Temporal-wise Attention Spiking Neural Networks for Event Streams Classification. In *2021 IEEE/CVF International Conference on Computer Vision (ICCV)*. 10201–10210. [doi:10.1109/ICCV48922.2021.01006](https://doi.org/10.1109/ICCV48922.2021.01006)

[66] Bojian Yin, Federico Corradi, and Sander M. Bohté. 2021. Accurate and efficient time-domain classification with adaptive spiking recurrent neural networks. *Nature Machine Intelligence* 3, 10 (01 Oct 2021), 905–913. [doi:10.1038/s42256-021-00397-w](https://doi.org/10.1038/s42256-021-00397-w)

[67] Jinsung Yoon, Donghyun Lee, Neungyun Kim, Su-Jung Lee, Gil-Ho Kwak, and Tae-Hwan Kim. 2023. A Real-Time Keyword Spotting System Based on an End-To-End Binary Convolutional Neural Network in FPGA. In *2023 IEEE Symposium in Low-Power and High-Speed Chips (COOL CHIPS)*. 1–3. [doi:10.1109/COOLCHIPS57690.2023.10121981](https://doi.org/10.1109/COOLCHIPS57690.2023.10121981)

[68] Chengting Yu, Zheming Gu, Da Li, Gaoang Wang, Aili Wang, and Erping Li. 2022. STSC-SNN: Spatio-Temporal Synaptic Connection with temporal convolution and attention for spiking neural networks. *Frontiers in Neuroscience* 16 (2022). [doi:10.3389/fnins.2022.1079357](https://doi.org/10.3389/fnins.2022.1079357)